To appear in: Iranian Journal of Earth Sciences (Iran J. Earth. Sci.)

E-ISSN: 2228-785X Print ISSN: 2008-8779

Received: 25 January 2024 Revised: 2 February 2025

Accepted: 25 February 2025

DOI: https://doi.org/10.57647/j.ijes.2025.16946

Original Research

Evaluating the Alteration Zones and Environmental Impacts in the Chore Nab Iron Mine, NW Iran

Parisa Shahkarami[1], Reza Zarei Sahamieh*[1], Mohammad Ebrahimi[2], Ahmad Ahmadi Khalaji[1], Ramin Sarikhani[1]

1. Department of Geology, Faculty of Science, Lorestan University, Khorramabad, Iran.

2. Department of Geology, Faculty of Sciences, University of Zanjan, Zanjan, Iran.

* Corresponding author: Zarei.r@lu.ac.ir

Abstract

This research focuses on investigating the alteration zones and environmental impacts of potentially toxic element pollution in the soil surrounding Chore Nab in the Tarom subzone. Based on field and petrographic evidence, the area exhibits six alteration zones in both plutonic and volcanic rocks. Pollution indicators, such as the Igeo index, reveal a moderate arsenic (As) concentration of 1.36. Enrichment factor (EF) values indicate moderate enrichment for Cd at 2.74, Cr at 2.38, and Mn at 2.45, with significant enrichment for As at 6.50. The pollution index (PI) indicates high arsenic pollution (3.86), while the

pollution load index (PLI) reflects poor soil quality. The results reveal that arsenic poses a significant environmental and health risk, with a high EF of 6.50 and a PI of 3.86. During the study, significant positive correlations were found between Co and Ni (0.876), V and Ni (0.793), Mg and Co (0.704), Cu and Cd (0.982), and Cu and Pb (0.805), suggesting a common origin, presence in sulfide minerals, or similar geochemical behavior among these elements in relation to one another. Moreover, multivariate statistical methods, including principal component analysis (PCA) and hierarchical cluster analysis (HCA), were employed for soil classification. PCA revealed three factors accounting for 77.70% of the variance: the first factor (43.34%) includes Ni, Co, As, Ca, Cu, Fe, Pb, V, and Cd; the second factor (23.52%) includes Zn and Mg; and the third factor (10.84%) includes Co and Mo, which control the quality of soil resources. Based on HCA analysis, four clusters were observed. The multivariate analyses suggest that the source of contamination is primarily natural, with human activities not contributing to additional pollution in the area. Pearson correlation and PCA indicate that the distribution of elements such as Cd, Fe, Ni, Cu, As, Pb, Ca, V, and Co is controlled by lithological sources, while the distribution of Zn and Mg is influenced by rock weathering and the alteration of mafic rocks.

Keywords: *Chore Nab; Alteration; Potentially toxic elements; Pollution indices; Principal Component Analysis.*

1. Introduction

The pollution of the natural environment by potentially toxic elements is a worldwide problem (Sobhanardakani, 2019). These elements have toxic effects even at low concentrations (Sikakwe and Ilaumo, 2023). They are highly toxic, with adverse ramifications on the human body, engendering a myriad of complications such as high blood pressure, damage to the nervous system, and bone diseases (Negahban and Mokarram, 2021). The presence of various contaminants such as As, Cd, Cr (III), Cr (VI), Cu, Mo, Ni, and Zn in both water and soil indicate that these elements can cause pollution (Mokarram et al., 2020). Alteration processes and weathering, which are natural geochemical transformations, can significantly change the chemical composition and mineralogy of the original rocks. These processes often lead to the release, concentration, or discharge of potentially toxic and non-metallic elements into the environment, affecting plants, animals, and humans (Mollai et al. 2014; Abdullah et al., 2015; Tajam and Kamal, 2013; Talaei et al., 2019; Nazari et al. 2023; Schaefer et al., 2023; Abdolahadi et al. 2025; Salehpour et al. 2025). These elements originate from both natural and anthropogenic sources, including the use of chemical and organic fertilizers and pesticides containing potentially toxic elements, mining, power generation, industrialization, urban development, waste spills, smelting, and fuel combustion, which are the most significant sources of metal emissions (Sabet Aghlidi et al., 2020; Ousta et al. 2024). Mining and mineral processing are two of the most critical sources of potentially toxic elements that enter the environment and contaminate various parts of the biosphere. Along with population growth and industrial progress, the dramatic expansion of mining activities for metal extraction has led to severe environmental issues around mines caused by metal pollutants. Accordingly, the discharge of tailings without observing environmental standards causes pollution of water, soil, air, and agricultural products. Consequently, metal pollutants find their way into the food chains of humans and animals (Kabata- Pendias, 2011; Münzel et al., 2023). Potentially toxic elements such as Pb, As, Zn, Cr, and Cd are among the most critical pollutants due to their toxic properties and potential for bioaccumulation. Additionally, they represent one of the most hazardous groups concerning toxicity and stability. These metals hold significant ecological and biological importance due to their long shelf life and accumulation in living tissues (Atabaki et al., 2018). Children are more vulnerable to these metals than adults due to their rapid growth and metabolism (Matta et al., 2016; Upadhyay et al., 2024; Simatupang et al., 2024).

These metals can enter the body through water, air, soil, and skin, eventually entering aquatic ecosystems (Lentini et al., 2017; Azami et al., 2018). Cobalt, an essential nutrient and an integral part of vitamin B12, is necessary for proper thyroid function and plays a crucial role in regulating blood pressure. Exposure to high amounts of this element can damage the lungs and heart and cause dermatitis. Nickel, at trace levels, plays a vital role in red blood cell synthesis and may be beneficial for activating certain enzyme systems. However, exposure to high content of nickel for an extended period may result in respiratory problems, damaged cells, liver and heart issues, lung cancer, damage to the nervous system, and decreased body weight. Vanadium can change between two oxidation states (V and IV) and can also bind to blood proteins. It should be noted that there are no available data on the carcinogenicity of V in humans (Sobhanardakani, 2019). However, exposure to high levels of Zn and Cu can lead to extensive lesions in the kidneys, nephritis, hair loss, inflammation in brain tissue, anorexia, panic attacks, migraines, anxiety, childhood hyperactivity, kidney and liver dysfunction, autism, and even cancer (Sabet Aghlidi et al., 2020). Zn enters the body through plants such as lettuce. Arsenic, as a carcinogenic agent, provides no benefits to living organisms, even at low levels. Anorexia, fever, hair loss, goiter, muscle spasms, decreased production of red and white blood cells, nausea, vomiting, and especially kidney and liver damage are the main consequences of exposure to arsenic. Although Cr (III) plays a vital role in the metabolism of macromolecules, hexavalent chromium (Cr (VI)), is a carcinogenic agent, and exposure to this element can cause adverse effects on human health, including nose ulcers, wheezing, shortness of breath, and asthma (Sabet Aghlidi et al., 2020). Cadmium and lead, as highly toxic elements even at low levels, can cause kidney injuries, reduced reproductive capacity, hepatic dysfunction, hypertension, and tumors. Moreover, hyperactivity, impaired hearing, and a reduction in children's IQ are the main effects of exposure to Pb (Sabet Aghlidi et al., 2020). Some elements, such as Mn and Fe, are essential and play functional and structural roles in biological systems. For example, Fe is a key component of hemoglobin (Mohebian et al., 2021). Selenium is a vital trace element for mammals. Through selenoproteins, this mineral participates in various biological processes, including antioxidant defense, thyroid hormone production, and immune response. Some reports indicate that a human organism deficient in selenium may be prone to certain diseases. Adverse health effects following selenium overexposure, although very rare, have been observed in both animals and humans (Zwolak and Zaporowska, 2012; Zhang et al., 2023).

One of the standard quantitative methods for calculating soil pollution is using environmental indices to determine the degree of pollution and the contributions from both natural and anthropogenic sources. In general, pollution indices are divided into two groups: individual indices and cumulative indices. Individual indices include the contamination factor (CF), enrichment factor (EF), and geoaccumulation index (I_{geo}). Additionally, cumulative indices include the Pollution Load Index (PLI). Individual indices examine the pollution of a single element or pollutant, while cumulative indices assess multiple metal pollutants (Qingjie et al., 2008; Tomczyk et al., 2023). These indices have been utilized in numerous studies across various countries to estimate pollution levels (Gong et al., 2009; Neeraj et al., 2023; Saadat et al. 2023). Few types of research on soil contamination analyzing toxic elements have been conducted in developing countries, particularly in Iran. For instance, one study examined the environmental impacts of iron ore mining and processing in the Chore Nab mine (Torkashvand et al., 2019). This research aims to assess ecological pollution based on pollution indices. It also investigates alteration zones and the release of toxic and heavy elements during alteration and mineralogical processes. To this end, the results of petrographic studies and geochemical analyses, including ICP-MS on the region's rocks, were utilized. While numerous studies have focused on environmental pollution, particularly soil contamination by potentially toxic elements, research on the specific impacts of alteration processes and mining activities in the Chore Nab iron mine is still limited. Previous studies have generally addressed the environmental impacts of mining in Iran (Torkashvand et al., 2019). By analyzing petrographic data and performing geochemical analyses (ICP-MS

and XRF) on regional rocks, this research provides novel insights into the release and concentration of toxic elements during alteration and mineralogical processes. Potentially toxic element contamination affects not only the physicochemical properties of soil, reduces biological activity, and decreases the bioavailability of soil nutrients, but also poses a serious threat to human well-being (Yazdi et al. 2015; Negahban et al., 2021). The findings indicate a significant environmental risk, particularly due to arsenic contamination, necessitating immediate remediation efforts. The moderate to significant enrichment of potentially toxic elements in the area poses a threat to local ecosystems and human health.

2. Geographical and geological setting of the study area

Chore Nab is a village located in the central part of Zanjan Province, Iran. The village is called Chore No by the locals and is known by its former name, Soleymanabad. The study area, covering approximately 20 km^2, is located 5 km northeast of Zanjan city, with geographical coordinates of 36° 41′ 10″ to 36° 43′ 40″ N and 48° 32′ 25″ to 48° 35′ 19″E (Fig. 1). This region has a cold climate in winter and a moderate climate in summer. In addition, in terms of structural land divisions, it is considered part of the Tarom magmatic zone. According to Tarom's 1:100,000 geological map (Hirayama et al., 1966; Stocklin et al., 1969; Amini, 1997), several rock units with outcrops are present in the study area. From old to new, these rocks are Eocene volcanic and pyroclastic rocks, including basalt, dacite, andesite basalt, andesite, sandstone and green tuff in the lower part (unit E^5k.a), light green tuff breccia and lapilli tuff (E^6k.a) and andesitic lavas with tuff breccia, green tuff, sandstone, and mudstone (unit E^8k.a). The Late Eocene granitoid rocks have a lithological composition of quartz monzodiorite, quartz monzonite, quartz syenite (unit qm), and microquartz diorite porphyry (unit P). Quaternary deposits consist of old alluvial terraces (unit Q_1^t) and new alluvial terraces (unit Q_2^t). Fig. 2 illustrates the geological map of the study area. Based on the field studies and petrographic data of the present research, the rocks found in this area can be categorized into three groups: volcanic rocks, plutonic masses, and Quaternary period deposits. A major part of the rock units identified in the study area is volcanic rocks (e.g., basalt, basaltic andesite, andesite, trachyandesite, and dacite) and granitoid plutonic rocks with the composition of granite, granodiorite, monzonite, quartz monzonite, quartz monzodiorite, and monzodiorite. Fig. 3 depicts the field view of igneous rocks with outcrops in the study area.

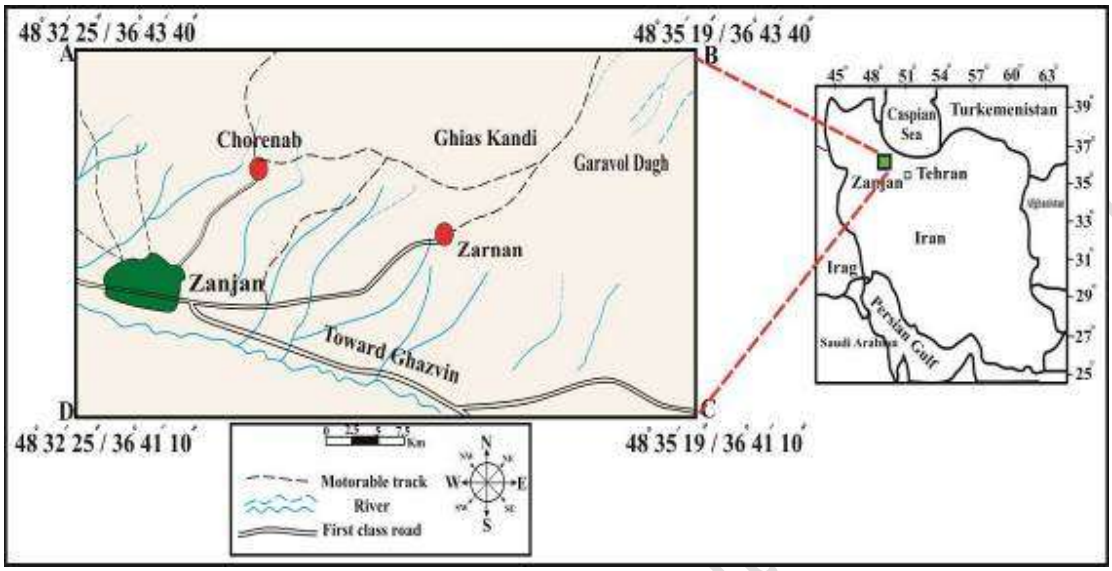

Figure 1. Map of access roads to the study area.

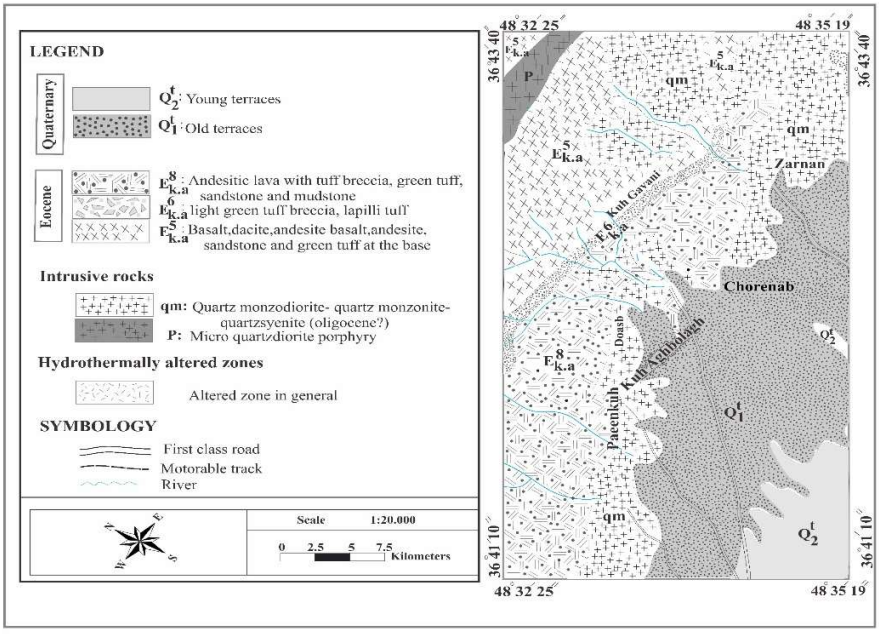

Figure 2. Geological map of the study area.

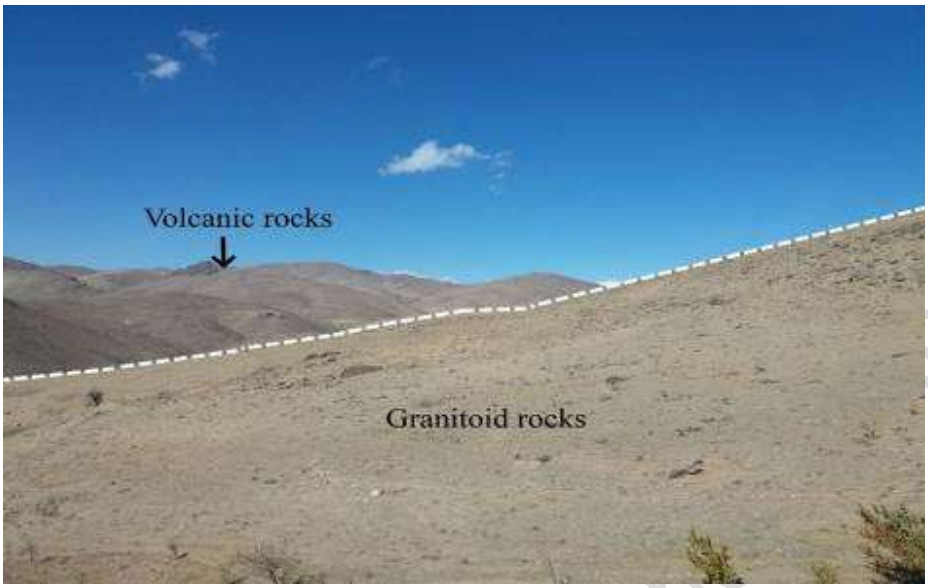

Figure 3. A view of the studied area where volcanic and granitoid rocks are separated (view of the image towards the east).

3. Materials and methods

3.1. Research Methodology

The rock units of the study area were visited for field sampling and surveys. Subsequently, 36 thin sections and 22 polished thin sections were prepared at Bu-Ali Sina University for petrographic studies, ore microscopy, and identification of alterations. Petrographic studies were conducted using a Leica polarized light microscope, while ore microscopic studies were performed with a Prior polarized light microscope. During petrographic and ore microscopic studies, fourteen samples were selected for whole rock chemical analysis. The selected samples were prepared and analyzed by Zar Azma Company in Tehran. They performed an inductively coupled plasma mass spectrometry (ICP-MS) method for rare earth elements and trace elements and the TXRF method for major oxides. Moreover, they conducted XRF analysis for major and minor oxides. Five samples of mineralized rocks and five samples of altered rocks were studied using field emission scanning electron microscopy (FE-SEM) and X-ray energy dispersive spectroscopy (EDS) analysis. SEM studies were conducted using the FE-SEM device model MIRA3-LMU at Lorestan University. Additionally, ten samples were selected for X-ray diffraction (XRD) studies and analyzed using an STADI P XRD device manufactured by STOE, Germany, at Lorestan University.

3.2. Petrography

During the field observations, various rock units were selected for sampling and petrographic surveys. Then, thirty-six thin sections and twenty-two polished thin sections were prepared to conduct petrographic, mineralogical, and alteration studies. Based on petrographic studies, various rocks, including basalt, basaltic

andesite, andesite, trachydacite, quartz monzonite, quartz monzodiorite, and monzodiorite, were identified in the region. The lithological characteristics of these rocks are briefly described in the following lines.

3.2.1. Basalt: Basalts often exhibit a porphyritic texture, characterized by large plagioclase and pyroxene crystals embedded within a fine-grained microlitic groundmass (Fig. 4a). Plagioclase microlites have a random orientation and do not exhibit any specific preferred orientation. The constituent minerals of these rocks are primarily plagioclase and pyroxene, with the abundance of plagioclase being significantly higher than that of pyroxene. Coarse plagioclase crystals display repeated twinning, and in some instances, they exhibit albite-Carlsbad twins. Some plagioclase crystals can reach a maximum size of 3 mm and show zoning features. Coarse pyroxene crystals are often subhedral and occasionally octagonal, with a maximum length of 1.5 mm.

3.2.2. Basalt andesite: These rocks have glomeroporphyritic (Fig. 4b) and porphyritic textures with large plagioclase and pyroxene crystals set in a fine-grained groundmass. The glomeroporphyritic texture results from the accumulation of plagioclase, amphibole, and pyroxene crystals. Plagioclase and pyroxene are the primary minerals of these rocks, existing in the form of microcrystals to coarse crystals. Repeated twins, and in some cases, albite-Carlsbad twins, are observed in large plagioclase crystals. The maximum size of plagioclase crystals reaches up to 2.5 mm, and they are sometimes zoned. Coarse pyroxene crystals are often subhedral and occasionally octagonal. The maximum size of pyroxenes can reach up to 1 mm, and in some instances, they exhibit mechanical twins. The amphibole crystals in these rocks are primarily subhedral, with a maximum size of 1 mm. Occasionally, the amphibole crystals are altered to chlorite.

3.2.3. Andesite: Andesite rocks have porphyritic and glomeroporphyritic textures. Large plagioclase, amphibole, and pyroxene crystals are embedded in a fine-grained matrix in these rocks. The glomeroporphyritic texture results from the accumulation of large plagioclase crystals in a fine-grained matrix (Fig. 4c). Plagioclase is the most abundant mineral in the rock and is mainly subhedral. Coarse plagioclase crystals exhibit zoning and repeated twinning, with albite-Carlsbad twins reaching a maximum size of 2.5 mm. Coarse pyroxene crystals are often subhedral and sometimes octagonal, with a maximum length of 1 mm. Amphiboles are typically subhedral, with the largest size reaching 1.5 mm.

3.2.4. Trachydacite: The dominant texture in trachydacite rocks is porphyritic. These rocks contain large feldspar crystals, including sanidine, and are set in a fine-grained matrix consisting of quartz, sanidine, plagioclase, and opaque minerals. Coarse sanidine crystals are subhedral and exhibit Carlsbad twinning (Fig. 4d). The maximum size of sanidine crystals in these rocks reaches 2.5 mm.

3.2.5. Quartz Monzonite: Quartz monzonite rocks have a granular texture and are somewhat altered (Figs. 5a and 5b). The main constituting minerals of these rocks are quartz, plagioclase, and alkali feldspars. The mafic minerals are pyroxene and amphibole, which decompose into secondary minerals, particularly chlorite. The mean size of the crystals forming these rocks is approximately 2 mm. Magnetite is a minor mineral in these rocks (Fig. 5a). In some cases, calcite veinlets or quartz-specularite veinlets cut through the rock (Fig.5b).

3.2.6. Quartz monzodiorite: Quartz monzodiorite rocks exhibit a porphyritic microgranular texture (Fig. 5d). The primary minerals in these rocks are quartz, plagioclase, and alkali feldspar, typically displaying anhedral and, less frequently, subhedral morphologies. The abundance of plagioclase in quartz monzodiorite exceeds that of alkali feldspar. Coarse plagioclase crystals in the rock often show repeated twinning and, on rare occasions, albite-Carlsbad twinning.

3.2.7. Monzodiorite: Monzodiorite rocks have a granular texture, and their main minerals include plagioclase and alkali feldspar (Fig. 5c). Plagioclase is often anhedral and sometimes subhedral. The mafic

minerals of the rock are pyroxene and amphibole, which are typically anhedral. The average size of the crystals in these rocks is approximately 3 mm. Magnetite is present as a minor mineral in these rocks.

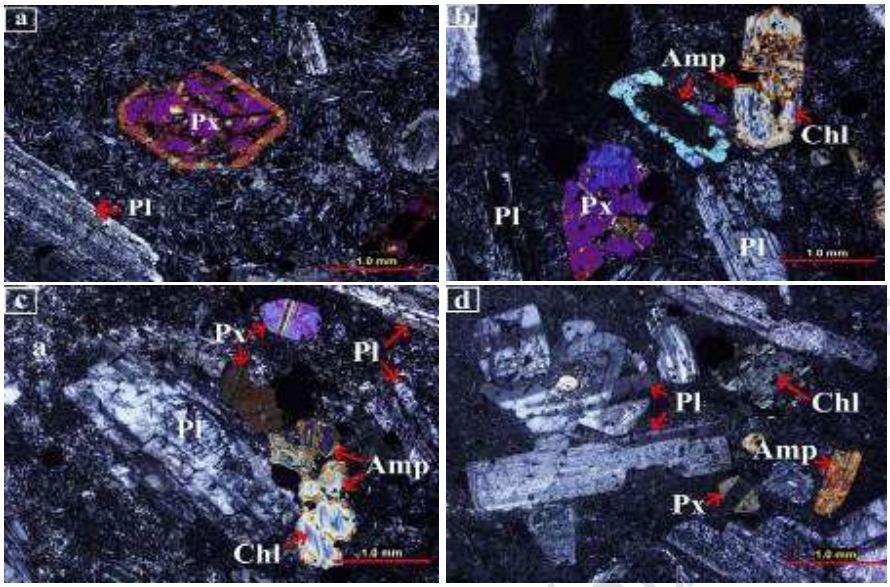

Figure 4. Microscopic images of the studied volcanic rocks (XPL light). a) Coarse crystals of pyroxene and plagioclase are found in basalt with a microlitic porphyritic texture. b) Basaltic andesite with a porphyritic texture. c) Andesite with a glomeroporphyritic texture. d) Trachydacite with a porphyritic texture. Mineral abbreviations are adapted from Whitney and Evans (2010). Px; pyroxene, Pl; plagioclase, Afs; alkali feldspar, Amp; amphibole, Chl; chlorite.

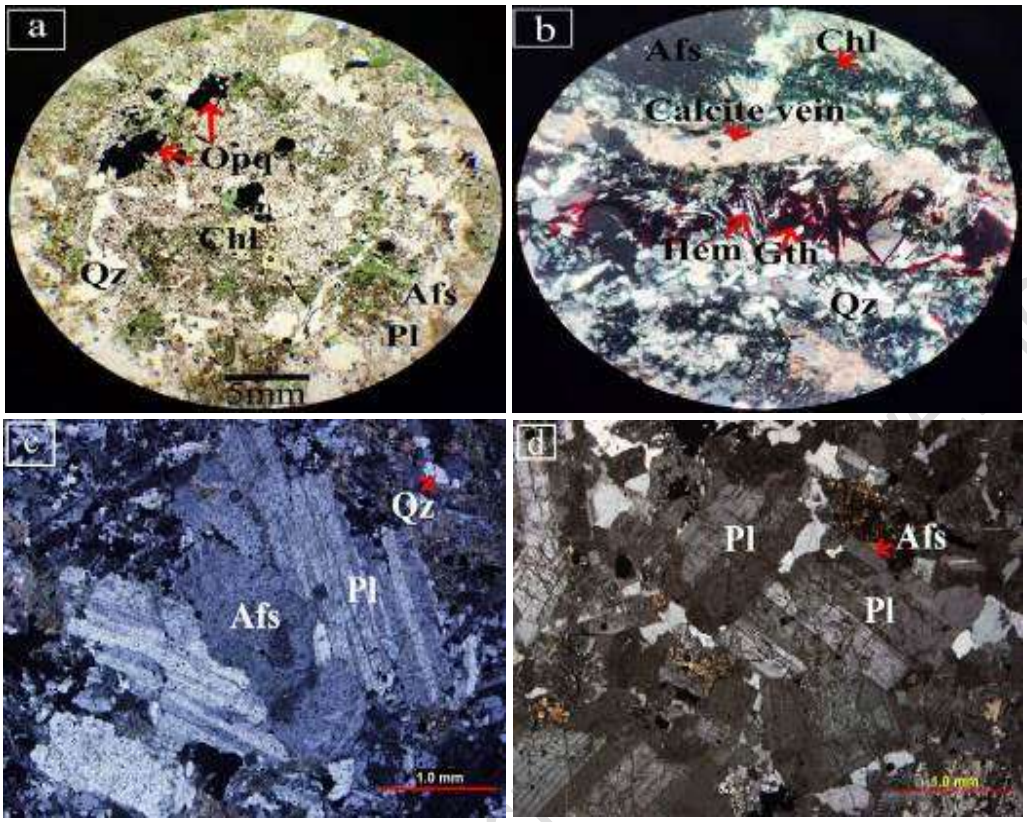

Figure 5. a) Quartz monzonite with a granular texture and chlorite alteration (PPL light). b) Carbonate alteration in the form of calcite veins cutting through quartz monzonitic rocks. The opaque crystals are lamellar hematite sheets (specularite) (XPL light). c) Granular texture in monzodiorite (XPL light). d) Quartz monzodiorite with a granular texture (XPL light). Mineral abbreviations are adapted from Whitney and Evans (2010). Qz; quartz, Pl; plagioclase, Afs; alkali feldspar, Chl; chlorite, Opq; opaque minerals and Hem; hematite. Ep; Epidote, and Cal; Calcite.

3.3. Alteration

In the Chore Nab area, alteration processes play a crucial role in the mineralogical and geochemical evolution of the ore body. The two primary types of alteration processes are hydrothermal alteration and weathering alteration, each affecting the deposit differently and resulting in the formation of distinct mineral assemblages (Pirajno, 2008). Hydrothermal alteration refers to the chemical alteration of minerals in rocks due to interaction with hydrothermal fluids, which are hot, chemically reactive water solutions (Bonyadi and Sadeghi, 2020; Chowdhury et al., 2024). This process typically occurs in areas of high temperature and pressure, such as near volcanic activity or in metamorphic environments. Hydrothermal alteration can lead to the formation of new minerals, such as sericite, chlorite, and epidote, which often indicate the presence of significant mineral deposits. The alteration of minerals during this process can also mobilize valuable metals, making hydrothermal systems important for ore genesis. In apatite-magnetite deposits,

hydrothermal alteration can significantly impact the concentration and distribution of ore and gangue minerals. Hydrothermal fluids can introduce or redistribute metals, enhancing the concentration of economically valuable minerals such as magnetite and apatite. This interaction between the fluids and the host rock can result in the recrystallization or replacement of existing minerals, including apatite, magnetite, actinolite, chlorite, epidote, sericite, and albite. Additionally, due to the alteration process, secondary minerals may form as vein-veinlets or fill the cavities of the rocks. The occurrence of hydrothermal alteration in the Chore Nab area is confirmed by the presence of quartz veins and veinlets, as well as epidote, calcite, actinolite, and chlorite, along with iron mineralization and their host granitoid and volcanic rocks. Based on field evidence and petrographic studies, the alterations detected in this area include epidote, chloritic, silicic, carbonate, actinolite, and sericitic alterations. Fig. 6 presents field photographs and hand samples of the detected alterations in Chore Nab mineralization. Weathering or supergene alteration involves the chemical and physical breakdown of rocks at or near the Earth's surface due to exposure to atmospheric conditions, water, and biological activity (de Oliveira and Imbernon, 1998; Sampaio et al., 2018). This process can lead to the leaching of certain elements and the formation of secondary minerals, including hematite, goethite, and limonite. Oxidation, exposure to oxygen, can oxidize iron-bearing minerals, changing their chemical state. In leaching, soluble components may be removed, concentrating residual minerals. Goethite and hematite typically form from the oxidation of magnetite and other iron-bearing minerals. Clay minerals such as kaolinite, form from the breakdown of silicate minerals. Secondary phosphates can form from the alteration of primary apatite. Weathering can lead to the mobilization of potentially toxic elements (PTEs) such as lead (Pb), arsenic (As), and cadmium (Cd) from mineral deposits into soils and water bodies. This mobilization can pose significant risks to ecosystems and human health, particularly in areas affected by mining activities.

In summary, hydrothermal alteration in apatite-magnetite deposits often enhances mineralization by introducing or concentrating ore minerals through fluid-rock interactions, while weathering typically modifies the deposit by oxidizing and leaching minerals, leading to the formation of secondary mineral assemblages. Both processes are integral to the geochemical evolution of these deposits and can significantly affect their economic viability.

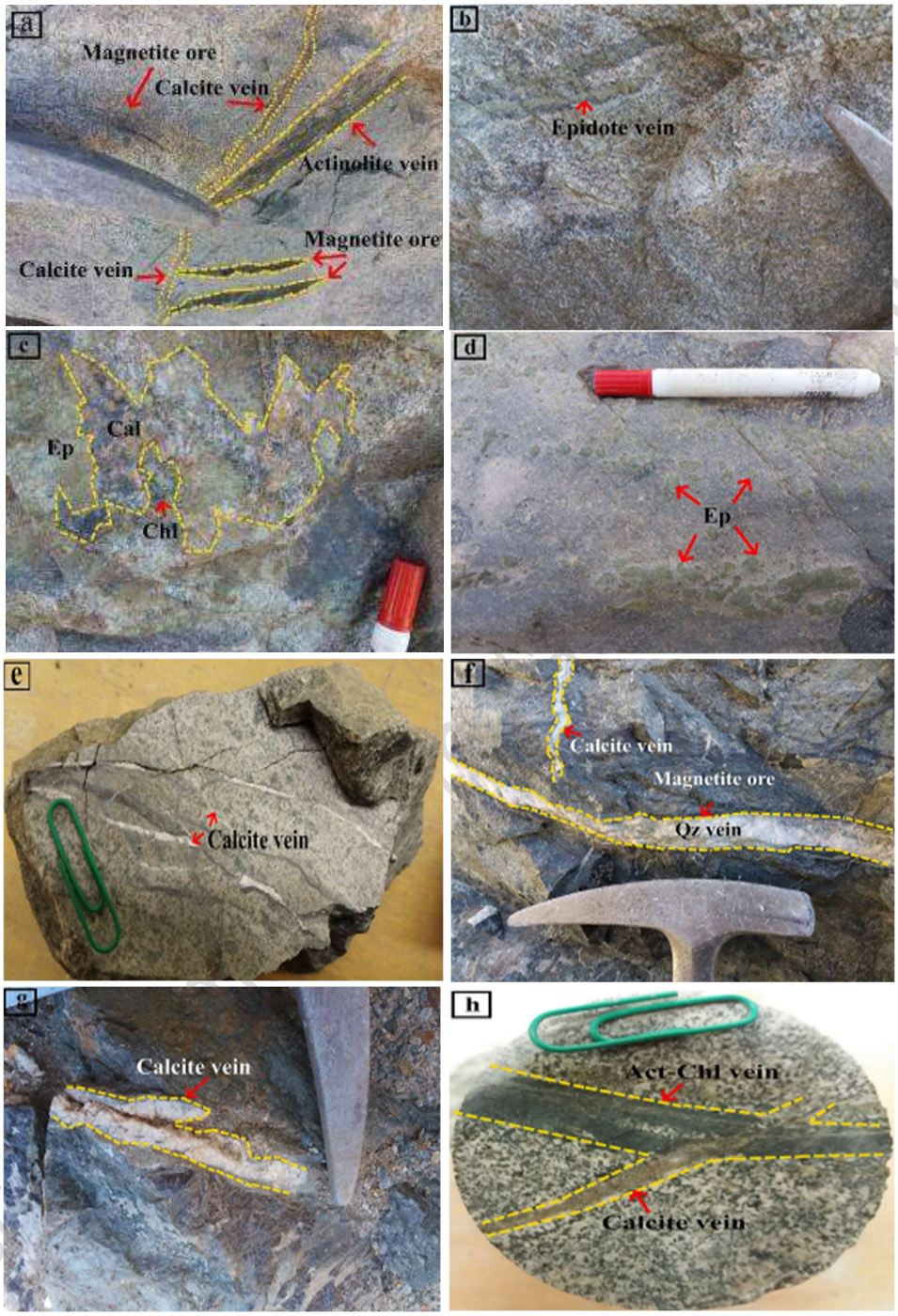

Figure 6. a) View of actinolite-calcite veins in granitoid rocks with iron mineralization. b) View of epidote alteration in granitoid rocks. c) View of epidote, calcite, and chlorite alteration in granitoid rocks. d) View of epidote alteration in volcanic rocks (basalt). e) Calcite veins in quartz-monzonite with a granular texture. f) View of silica veins in granitoid rocks. g) View of calcite veins with actinolite in granitoid rocks. h) View of calcitic and chlorite-actinolitic veins in a monzonite with a granular texture in granitoid rocks. Calcite

veins and chlorite-actinolite veins cut the host rock. Mineral abbreviations are adapted from Whitney and Evans (2010). Ep; epidote, Qz; quartz, Act; actinolite, Cal; calcite, and Chl; chlorite.

3.3.1. Silicic alteration

Silicification refers to an increase in the silica proportion in the form of quartz, chalcedony, and opal minerals, along with a decrease in the amounts of P2O5, K2O, CaO, and LOI in altered rocks. This phenomenon is attributed to precipitation from hydrothermal solutions or alteration of the glass of rocks and other minerals during leaching. Notably, different minerals may develop in the alteration halos (Li et al., 2013; Siani and Lentz, 2022). In the study area, silicic alteration can be observed on a microscopic scale as fine veinlets with low thickness filling the cavities in granitoid rocks. The microscopic and SEM images show that the silicic veinlets have cut through the granitoid host rock (Fig.7).

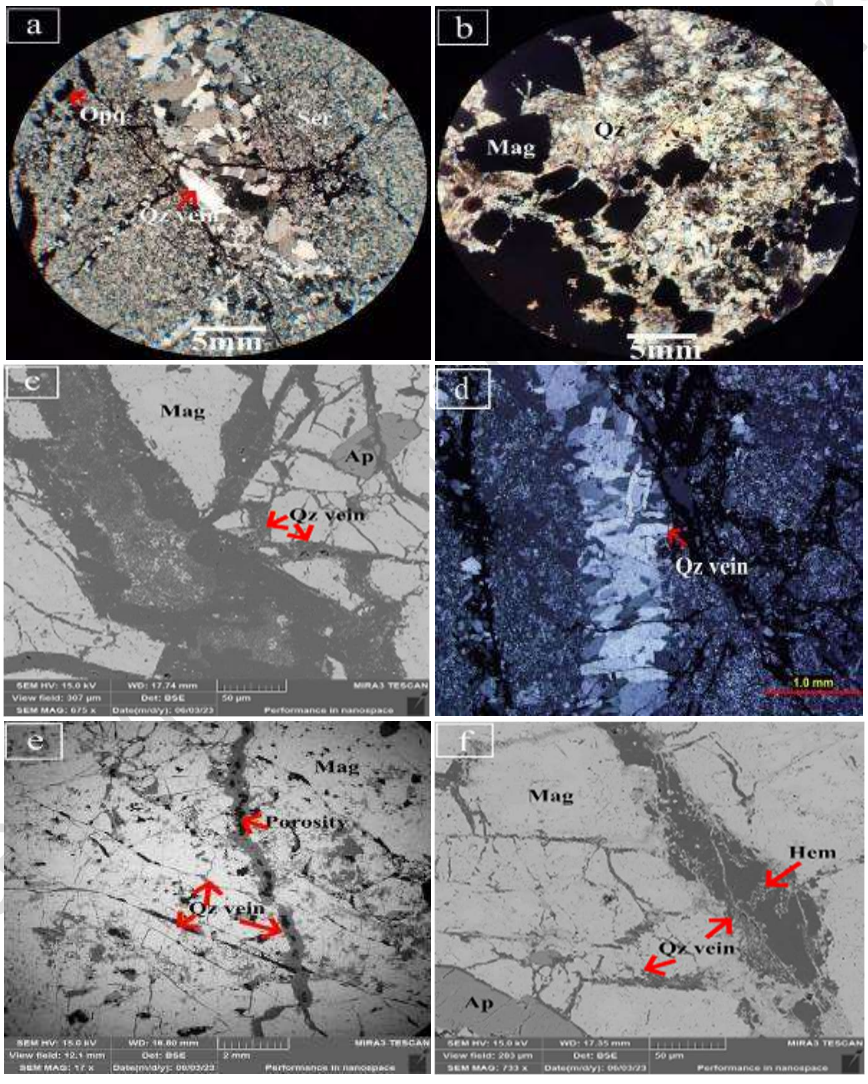

Figure 7. a) Silica vein that has cut a background consisting of alkali feldspar and sericite (PPL light). b) Quartz and chalcedony with scattered grains of magnetite (XPL light). c) SEM image of stockwork silica veins that have cut magnetite-apatite mineralization. d) Siliceous vein with comb

texture that cuts dacitic tuff (PPL light). e) Silica veins that have cut massive magnetite. f) Siliceous veins that have cut magnetite-apatite mineralization. Mineral abbreviations are adapted from Whitney and Evans (2010). Qz; quartz, Ser; sericite, Ap; apatite, Mag; magnetite, Hem; hematite and Opq are opaque minerals.

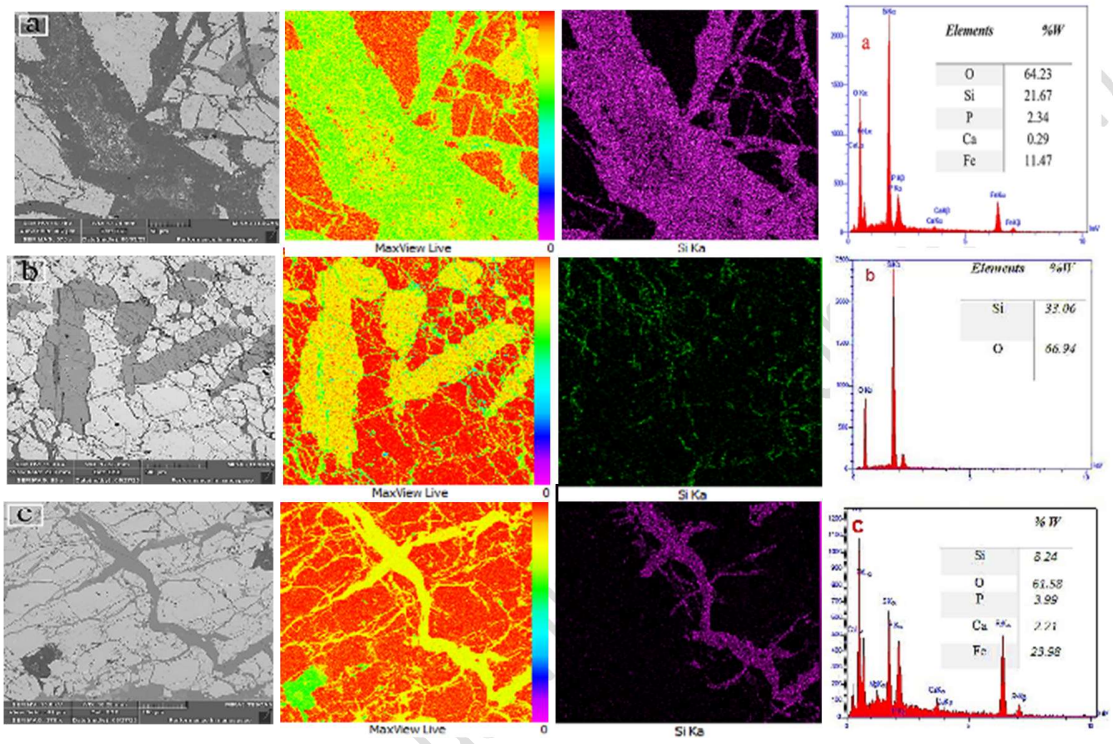

Figure 8. a) EDAX analysis of silica alteration, along with the weight percentage and distribution pattern of elements (Map), shows that Fe is related to magnetite ore, while Ca and P are associated with apatite. b) EDAX analysis of silica veins that have intersected apatites and magnetites. c) Stockwork silica veins that have intersected magnetite-apatite mineralization.

3.3.2. Carbonate alteration

Carbonatization produces carbonate minerals such as calcite, dolomite, magnesite, and siderite. This process occurs due to the alteration of a rock by solutions containing a high partial pressure of carbon dioxide (PCO_2) at alkaline pH. The formation of each type of carbonate mineral is controlled by the chemical composition of the fluids and the host rock (Robb, 2005; Bain et al., 2020). In the studied area, this type of alteration manifests as calcite veins and veinlets cutting through the granitoid rocks (Figs.9 and 10).

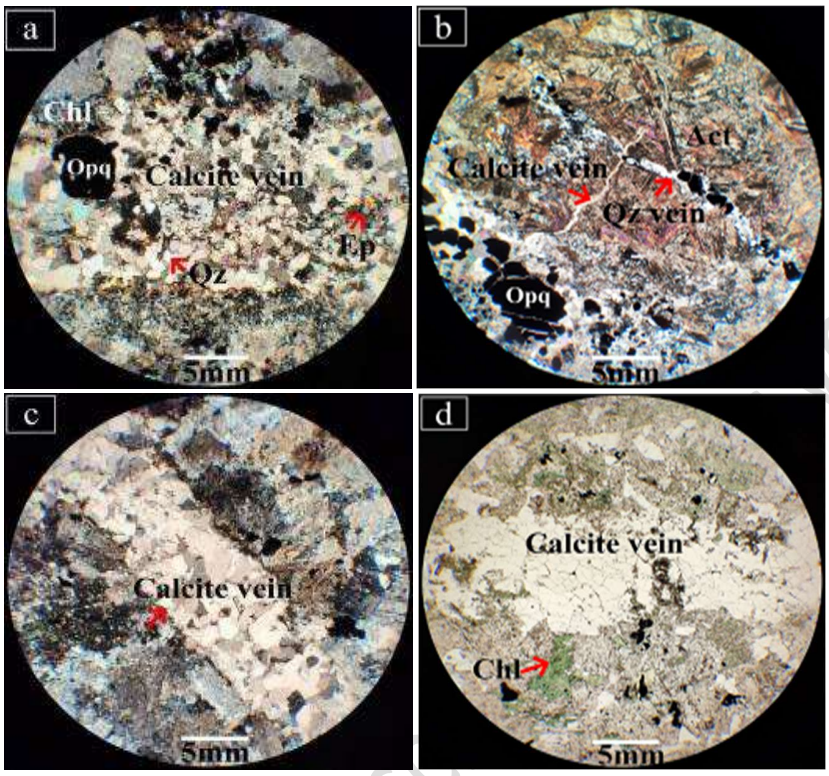

Figure 9. a) Calcite vein that has cut monzonite with a granular texture (XPL light). b) thin calcite vein intersects quartz vein and actinolite-quartz assemblage (XPL light). c) Veins of calcite with a mosaic texture cutting quartz monzonite with a granular texture (XPL light). d) Calcite vein with a mosaic texture in quartz monzonite, exhibiting a granular texture. In the background of the rock, chlorite is visible in green color (PPL light). Mineral abbreviations are adapted from Whitney and Evans (2010). Qz; quartz, Act; actinolite, Ep; epidote; Chl; chlorite, and Opq; opaque minerals.

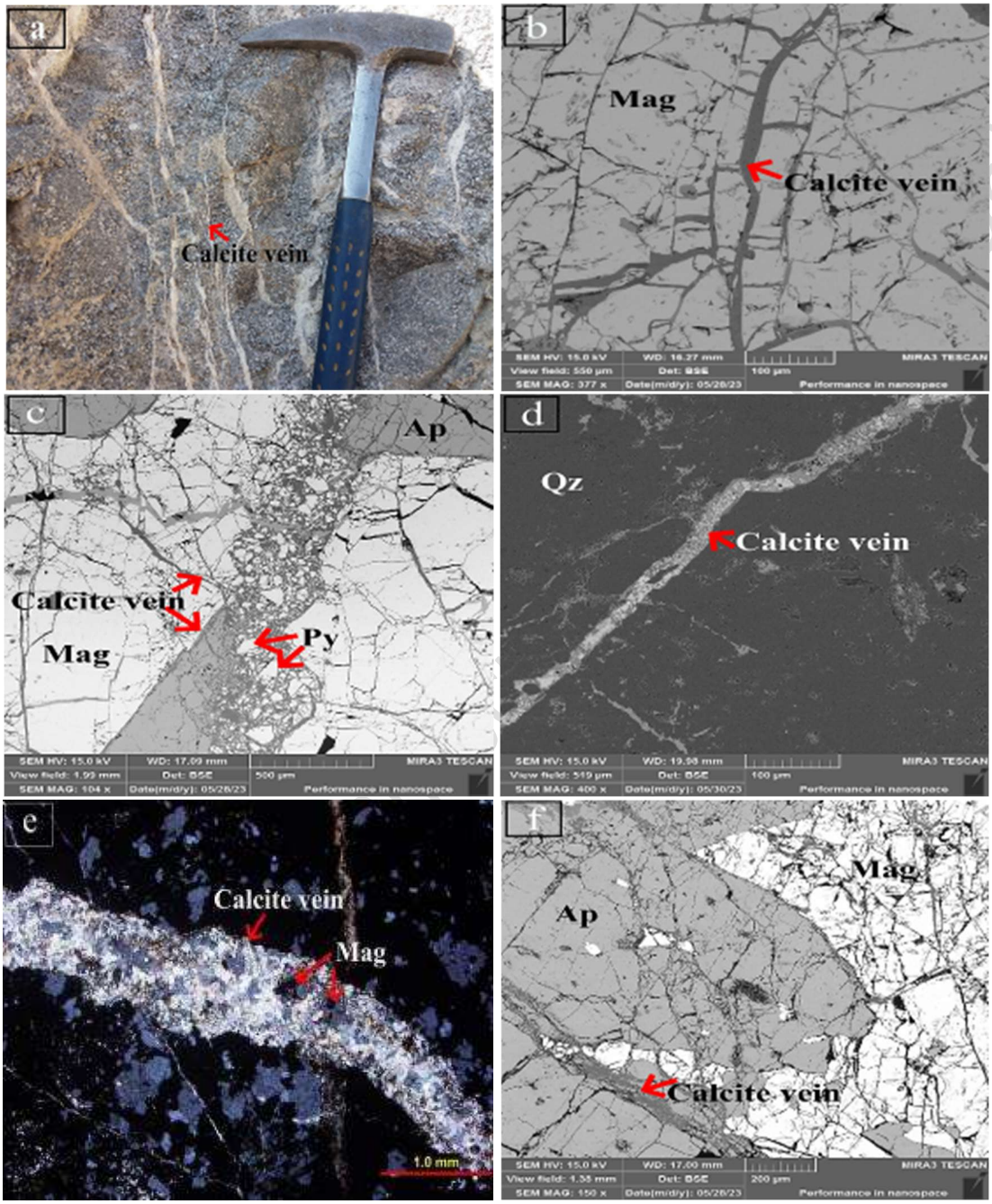

Figure 10. a) Close-up view of calcite veins in the studied volcanic rocks. b) SEM image of stockwork veinlets of calcite that have cut through magnetite. c) Stockwork calcite veins that have cut through the apatite-magnetite assemblage. In addition, pyrite is associated with calcite. d) The calcite vein has cut through the groundmass composed of quartz. e) Calcite vein cutting through the quartz-magnetite background (XPL light). f) SEM image of calcite veins that have cut through

apatite-magnetite mineralization. Abbreviations of minerals are adapted from Whitney and Evans (2010). Mag; magnetite, Ap; apatite, Qz; quartz, Py; pyrite, and Gth; goethite.

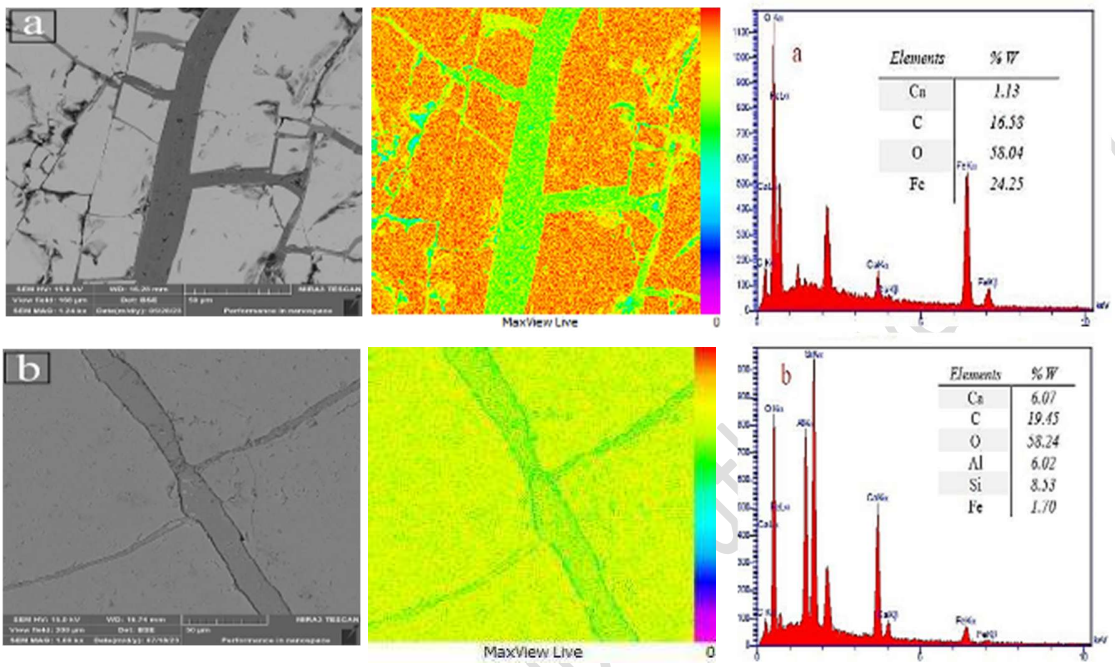

Figure 11. a) EDAX analysis of stockwork calcite veins intersecting magnetite. b) Analysis of stockwork calcite veins that have cut through epidote.

3.3.3. Chloritic alteration

Chloritization is a specific type of propylitic alteration characterized by a high percentage of chlorite. This alteration is often associated with sericitization. During hydrothermal alteration, chlorite is formed through substitution in ferromagnesian minerals, volcanic glass, or within cavities and fracture surfaces (Rae et al., 2011). The chlorite mineral is formed through: 1) the hydrothermal alteration of mafic minerals such as amphibole and biotite, and in some cases, pyroxene in igneous rocks; 2) the introduction of Fe and Mg into the rock through the penetration of hydrothermal fluids; and 3) a combination of both processes (Evans, 1992; Fan et al., 2021). In the study area, chlorite is the product of the decomposition and alteration of amphibole and biotite, and it is observed with an anomalous blue interference. In the field, it is also seen as veins and veinlets alongside actinolite (Figs.12 and 13).

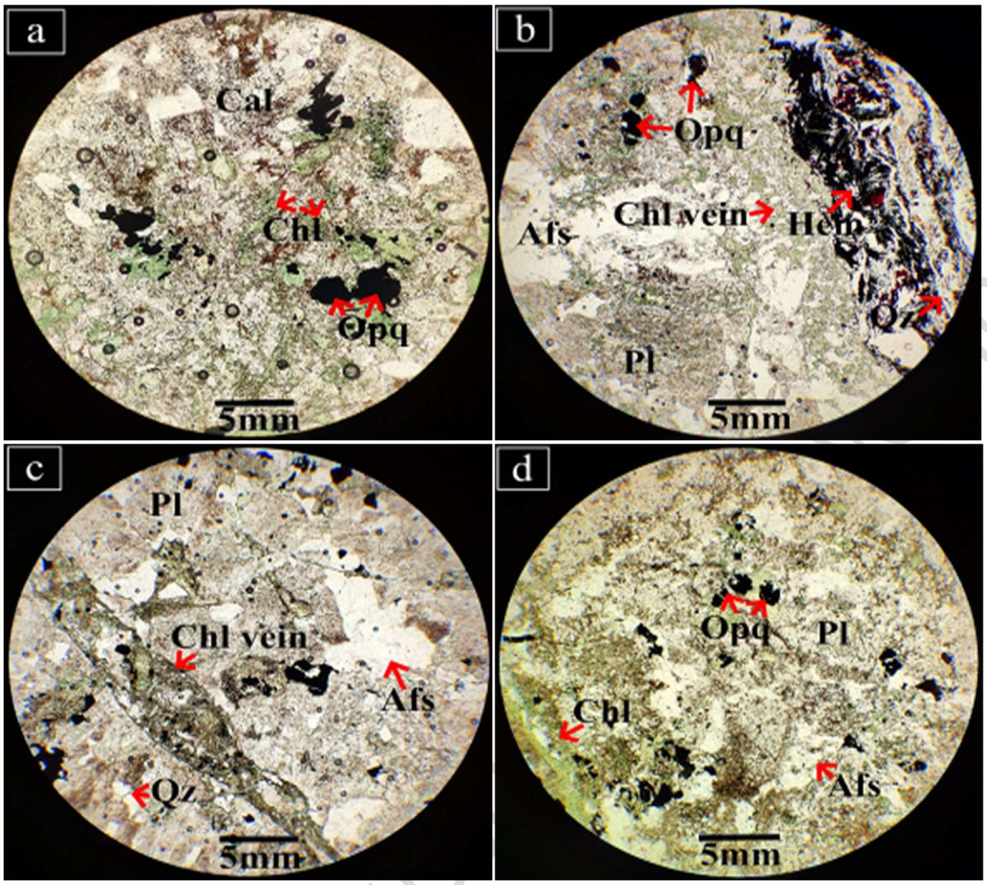

Figure 12. a) Chlorite alteration in an altered granite with a granular texture (PPL light). b) Chlorite alteration in a granular granite that has been cut by specularite veinlets (PPL light). c) The chlorite vein that has cut through granular quartz monzonite (PPL light). d) Chlorite alteration in quartz monzonite with a granular texture (PPL light). Mineral abbreviations are adapted from Whitney and Evans (2010). Qz; quartz, Pl; plagioclase, Afs; alkali feldspar, Chl; chlorite, Cal; calcite, Hem; hematite, and Opq; opaque minerals.

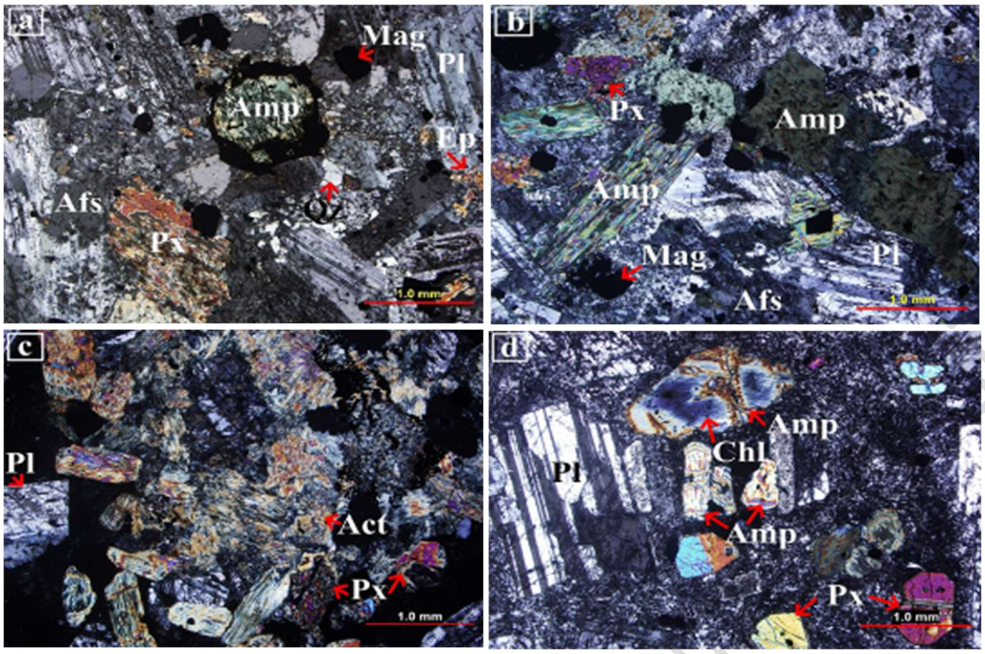

Figure 13. Microscopic images of the studied igneous rocks (XPL light). a and b) Occurrence of chlorite alteration in quartz monzonitic rocks with the conversion of amphibole to chlorite. c) Conversion of amphibole to chlorite (chlorite alteration) in basalt with a glomeroporphyritic texture and a glassy background. d) Conversion of amphibole to chlorite (chlorite alteration) in basalt with a microcrystalline background. Mineral abbreviations are adapted from Whitney and Evans (2010). Qz; quartz, Pl; plagioclase, Afs; alkali feldspar, Chl; chlorite, Px; pyroxene, Amp; amphibole, Mag; magnetite, and Ep; epidote.

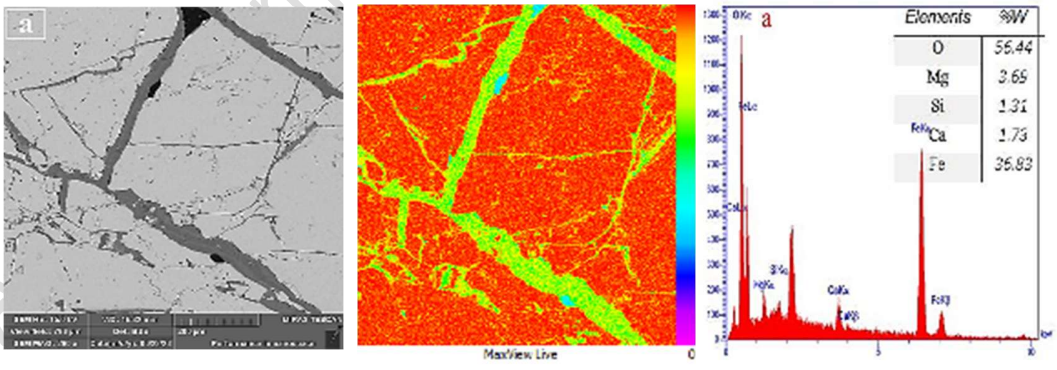

Figure 14.a) EDAX analysis of stockwork actinolite-chlorite veins that have cut massive magnetites.

3.3.4. Epidotic alteration

In epidotization, epidote is generated due to the alteration of plagioclase and hornblende (Hunstman, 1984; Wu et al., 2024). Epidote is often associated with chlorite in igneous rocks and results from the decomposition of minerals such as amphibole, pyroxene, and feldspar. In the study area, epidote is present in volcanic rocks, particularly basalt, due to the decomposition of minerals or within rock cavities. In plutonic rocks (including quartz monzonites and monzonites), epidote is observed as veins and veinlets (Fig. 15).

3.3.5. Sericitic alteration

In mineralogy, sericitization (phyllic alteration) refers to the alteration of quartz, sericite, and pyrite. In this alteration, plagioclase is replaced by sericite, quartz, pyrite, and clay minerals. With the consumption of plagioclase, the amount of CaO decreases during the reaction (Li et al., 2013; Biabangard et al., 2017). The essential minerals of sericitization in the study area are sericite and quartz, with sericite being more abundant than quartz (Fig.17).

3.3.6. Impact of alteration zones on the distribution of potentially toxic elements

The identified alteration zones in the Chore Nab region have distinct impacts on the distribution and concentration of potentially toxic elements. Epidotization enhances the concentration of iron and trace elements by incorporating them into epidote minerals. Chloritization results in elevated levels of magnesium and nickel due to chlorite's adsorption properties. Sericitization affects potassium and aluminum concentrations, reflecting the retention of these metals by sericite. Carbonatization leads to higher concentrations of calcium and lead as carbonate minerals stabilize these metals. Silicification increases silicon and aluminum levels, with metals trapped within quartz and silicate minerals. Finally, goethitization concentrates arsenic and cadmium through adsorption and incorporation into goethite. These findings demonstrate the significant influence of alteration processes on the distribution of potentially toxic elements in the study area.

Another method to detect alteration zones is to use graphs of MgO vs. SiO_2 variations and K_2O vs. SiO_2 variations (Fig.18). For this purpose, the data were normalized in SPSS software using basic charts (Leitch and Lentz, 1994).

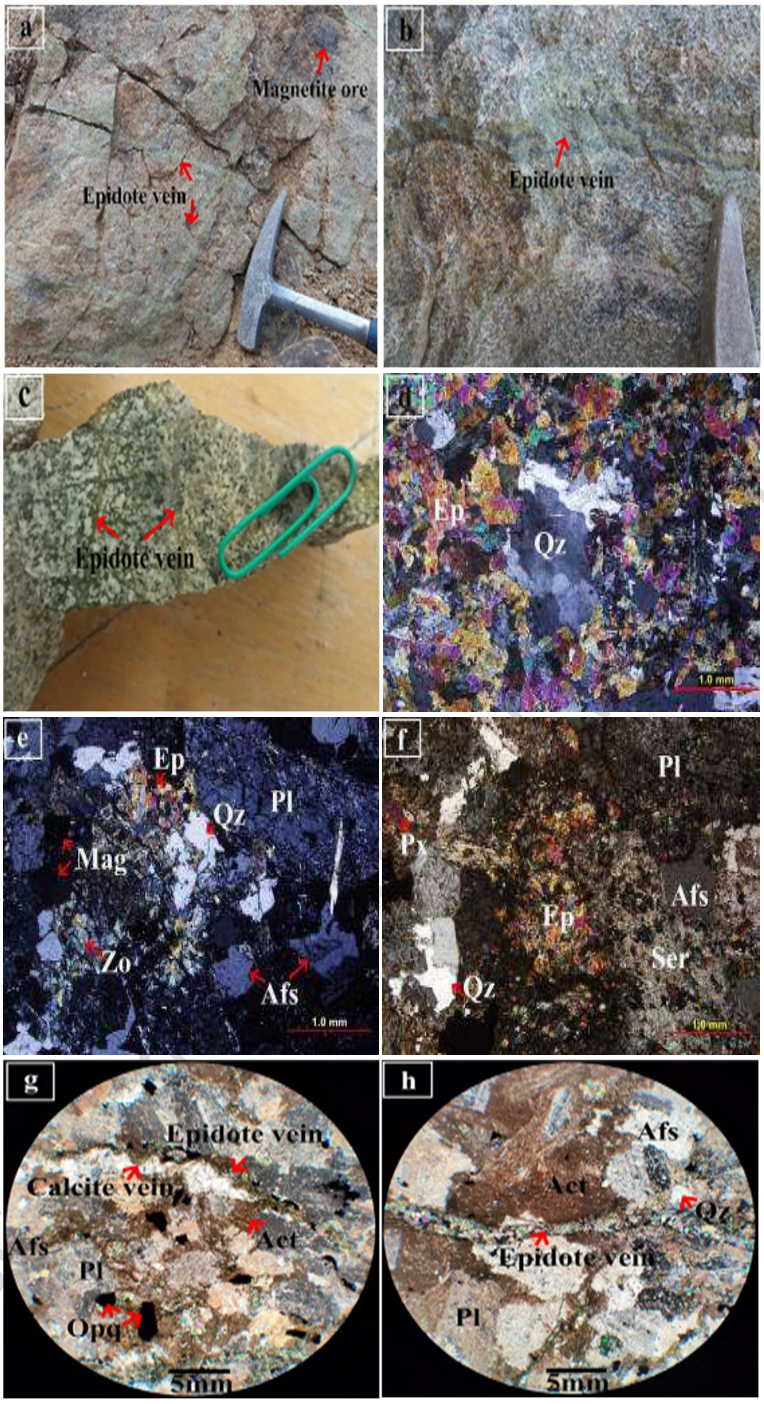

Figure 15. a) Epidote veins in granitoid rocks with iron mineralization. b) Epidote vein that has cut through the granitoid rocks. c) Epidote veins that have cut through granular quartz monzonitic rocks. d) Association of epidote and quartz (XPL light). e) Epidote alteration in a granular granodiorite (XPL light). f) Epidote alteration in quartz monzonitic rocks (XPL light). g) Epidote-calcite veins in granular quartz monzonite (XPL light). h) Epidote vein in quartz monzonite with

a granular texture (XPL light). Mineral abbreviations are adapted from Whitney and Evans (2010). Qz; quartz, Pl; plagioclase, Afs; alkali feldspar, Px; pyroxene, Amp; amphibole, Mag; magnetite, Ep; epidote, Ser; sericite, and Cal; calcite.

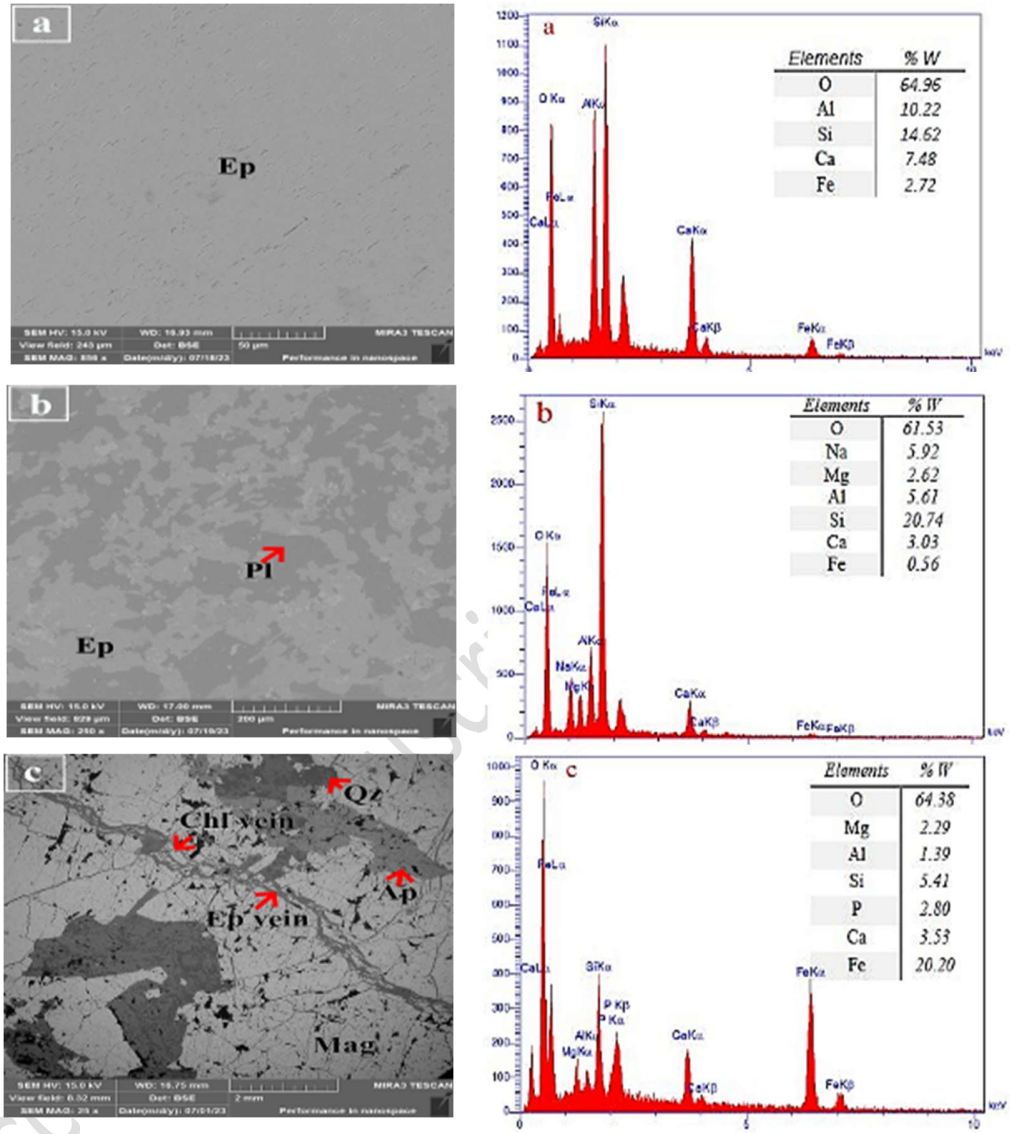

Figure 16. a) EDAX analysis of epidote. b) EDAX analysis obtained from sodic plagioclases transforming into epidote and chlorite. c) EDAX analysis of the epidote-chlorite vein cutting through the magnetite-apatite mineralization.

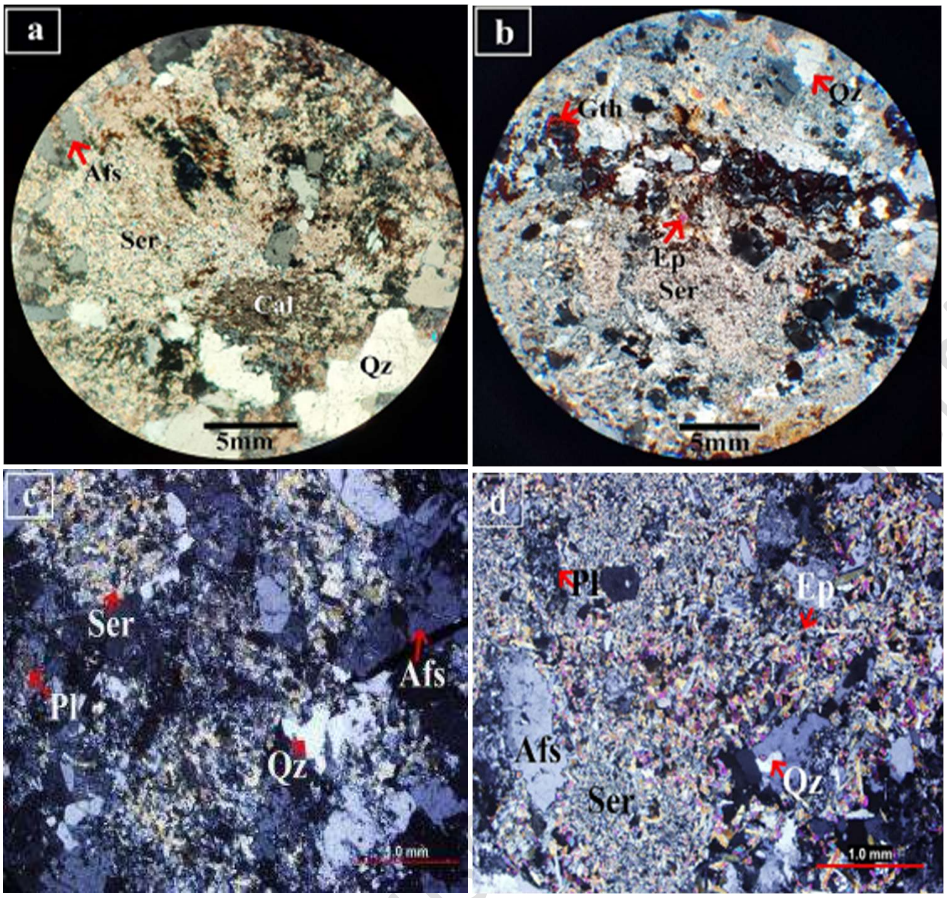

Figure 17. Microscopic images of sericite alteration in the studied granitoid rocks (XPL light): a and b) In quartz monzonite. c) In granular granodiorite. d) In granular granite. e and f) In granodiorite porphyry. Mineral abbreviations are adapted from Whitney and Evans (2010). Qz; quartz, Pl; plagioclase, Afs; alkali feldspar, Px; pyroxene, Ep; epidote, Ser; sericite, Cal; calcite, Gth; goethite, and Opq; opaque minerals.

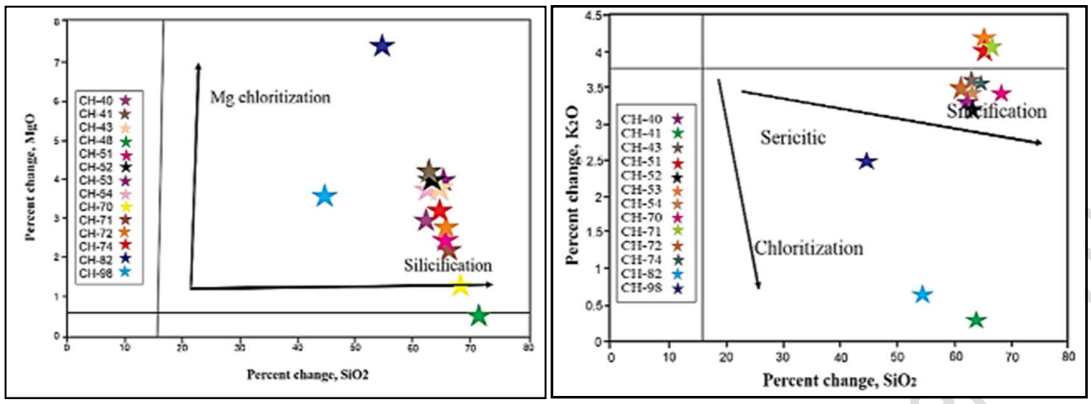

Figure 18. Geochemical methods to identify the effects of hydrothermal alteration by mass balance method (Leitch and Lentz, 1994).

3.4. Environmental Geochemistry

The geochemical characteristics of the rocks were investigated by selecting 14 out of the 50 samples collected from the study area. They were then sent to Zarazma Company for ICP-MS analysis. The alteration zones were determined in detail by selecting ten samples (five volcanic rock samples and five plutonic igneous rock samples) from the highly altered samples, which were subsequently analyzed using X-ray diffraction (XRD). For chemical analysis, fourteen samples were chosen to provide a comprehensive representation of the different rock types and alteration zones in the study area. These samples included a range of plutonic and volcanic rocks, selected based on their geological context and the observed alteration processes. The goal was to capture variations in metal concentrations across different alteration types and mineralization features. In this study, Inductively Coupled Plasma Mass Spectrometry (ICP-MS) was chosen to analyze rare earth elements and other trace elements due to its high sensitivity, low detection limits, and capability to analyze multiple elements simultaneously (Table 1). ICP-MS is particularly advantageous for detecting low concentrations of rare earth elements and trace metals, which are crucial for understanding the geochemical characteristics of the study area. The method's high throughput and precision ensure reliable and reproducible results across a broad dataset, making it well-suited for comprehensive geochemical analyses in environmental and mineralogical studies.

For X-ray diffraction (XRD) studies, ten samples were selected to represent significant mineralogical variations and alteration features observed in the study area. The selection focused on samples with distinct mineral assemblages or notable alteration features, ensuring a thorough characterization of alteration minerals. The number of XRD analyses was determined by practical considerations, including sample availability and analytical capacity.

3.4.1. Soil quality assurance (QA) and quality control (QC)

In this study, QA and QC procedures were conducted using duplicate samples. To assess the reproducibility of our results, duplicate field samples were collected simultaneously from the same location and in the same

manner as the other field samples. Duplicate field samples provided information on the repeatability of the sampling and analytical procedures. The analytical results from duplicate samples fell within accepted analytical limits.

3.4.2. Statistical analyses

All analyses were conducted using SPSS software. The means and standard deviations (SD) of the metal contents were calculated for each sampling site. The Kolmogorov-Smirnov (K-S) test was used to assess the normality of the data. Additionally, correlations between the elemental contents of soil samples were calculated using Pearson's correlation coefficient. Subsequently, principal component analyses (PCA) were conducted to identify the contamination sources, and PCA and hierarchical cluster analysis (HCA) were used to distinguish the different groups of elements. In multivariate statistics, a scree plot is a line plot of the eigenvalues of factors or principal components in an analysis. The scree plot determines the number of factors to retain in an exploratory factor analysis (FA) or the number of principal components to keep in a principal component analysis (PCA). According to this plot, three factors played the most important role in the pollution value, which is consistent with the results of the PCA.

3.4.3. Soil pollution assessment indices

Different indices have been presented to evaluate the degree of soil pollution. These indices are used to determine the presence or absence of soil contamination. In this study, ICP-MS results were used to evaluate these indices. In general, pollution indices are divided into two groups: individual indices and cumulative indices. In individual indices, a reference value is used to express the intensity of pollution. In almost all individual pollution indices, the desired degree of pollution is evaluated by measuring the amount of the target or selected element against a reference value or the amount of that element in the reference environment. Comprehensive or cumulative indices of pollution are used to examine several elements together. These indices are primarily calculated using the individual indices. In the Chore Nab region, both metallic and non-metallic minerals are abundant. The weathering and alteration processes in this region cause the decomposition of minerals and the release of metals into the water resources and sediments, leading to their transfer into the environmental cycle. For instance, the actinolite mineral (a type of asbestos, due to its fibrous nature) is released through alteration, thereby introducing it into the environmental chain. Asbestos inhalation is harmful and carcinogenic to human health. In addition, iron extraction in the Chore Nab mine is conducted through an open pit, which can produce dust that has detrimental environmental effects on miners and local residents. Notably, deficiency of this element is commonly found in mountainous areas far from the sea. This element is present in sulfide minerals, limestone, and volcanic rocks. Therefore, understanding the extent of metal pollution is crucial for reducing pollution and protecting people from its dangers. Metal mines and mining activities are among the sources of potentially toxic element pollution. Consequently, after flowing into rivers, the effluents from mining processes transport these toxic metals, introduce them to the ecosystem, and cause pollution. The potentially toxic elements remaining in sediments are absorbed by plants and the tissues of living organisms, through which they ultimately enter the human food chain. Based on the data obtained from ICP-MS analysis, the enrichment factor (EF), pollution index (PI), Nemerow pollution index ($PI_{Nemerow}$), contamination factor (CF), pollution load index(PLI), geo-accumulation index (I_{geo}), the sum of pollution index (PI_{Sum}), average pollution index (PI_{avg}), pollution index vector coefficient (PI_{Vector}), degree of pollution (C_{deg}), and multi-element pollution (MEC) were calculated for Se, As, Ca, Mg, Cd, Co, Cr, Cu, Mn, Mo, Ni, Pb, Zn, Fe, and V.

Table1. Results of ICP- MS analysis of soil samples from the Chore Nab region (in ppm).

Samples	Elements														
	Se	As	Ca	Mg	Cd	Co	Cr	Cu	Mn	Mo	Ni	Pb	Zn	Fe	V
CH-40	5000	1.2	36104	13219	0.29	13.2	22	93	938	1.08	10	39	90	39323	132
CH-41	5000	6.8	32384	16860	0.28	10.1	35	6	1844	0.66	12	24	218	38970	178
CH-43	5000	4.8	30640	17075	0.24	18.5	32	21	812	0.68	12	15	123	43593	162
CH-48	5000	20.9	91666	2710	0.31	4	172	9	2282	<0.5	8	29	21	59384	239
CH-51	5000	1.1	29541	11566	0.21	7.9	22	40	2721	0.51	8	17	82	41131	88
CH-52	5000	1.1	38092	17390	0.22	18.6	53	48	1022	0.84	14	16	80	46183	162
CH-53	5000	1.1	37379	17324	0.2	18.7	48	84	997	0.93	15	22	82	46024	159
CH-54	5000	1.1	35365	17407	0.26	19.3	50	29	1234	0.99	18	21	114	46786	167
CH-70	5000	0.7	24802	7081	0.25	9	14	39	373	0.69	11	15	65	30589	57
CH-71	5000	1.1	24995	11301	0.23	12.2	229	29	1488	0.64	9	18	57	42107	104
CH-72	5000	1.1	29486	13275	0.21	9.8	27	26	1329	0.51	8	17	72	39693	113
CH-74	5000	1.2	28906	14658	0.22	10.3	27	48	2634	0.64	7	29	116	45443	92
CH-82	5000	0.9	21817	>2%	0.22	15.7	121	24	1332	0.79	12	22	60	80009	137
CH-98	5000	16.4	65195	15583	1.4	27.5	103	712	1180	0.67	28	53	121	>10%	402

3.4.3.1. Quantitative calculations to determine soil Potentially Toxic Elements contamination

3.4.3.1.1. Enrichment Factor (EF)

EF is a suitable tool to separate the natural and anthropogenic origins of the pollution phenomenon (Sutherland, 2000; Ghassemi Dehnavi et al.,2019., Agyeman et al., 2023). This factor is used to determine possible natural or human sources of metals in dust particles and to assess the degree of potentially toxic element contamination. This index is determined by considering a reference immobile element not affected by human activities, e.g., Fe, Al, Li, Sc, Zr, and Ti. A reference element is one that changes slightly in the environment, and its concentration is not affected by human activities. In this study, Ti was considered the reference element, where [Cn/Cr]sample is the current concentration of the selected element to the concentration of the reference element in the sample, and [Cn/Cr] Reference denotes the current concentration of the desired element to the concentration of the reference element in the Earth's crust.

$$EF = \frac{(C_n/C_r)Sample}{(C_n/C_r)\,Reference} \quad \text{(Eq. 1)}$$

In this study, fifteen elements were examined. The higher the value of the EF, the more significant the contribution of human factors to the increase in pollution of the targeted metals in the region's soil.

3.4.3.1.2. Pollution index (PI)

$$PI = \frac{Ci}{C_{ir}} \quad \text{(Eq. 2)}$$

C_i is the concentration of the investigated element in the sample, and C_{ir} is the investigated component of the reference sample.

3.4.3.1.3. Nemerow Pollution Index ($PI_{Nemerow}$)

This index was used to assess the level of pollution risk and the awareness of pollution potential. The advantage of this index over other indices is that it determines the risk of contamination for all metals studied. This index is obtained using the following relationship:

$$PI_{Nemerow} = \sqrt{\frac{(\frac{1}{n}\sum_{i-1}^{n} PI)^2 + PI_{max}^2}{n}} \quad \text{(Eq. 3)}$$

Where PI is the pollution index, PImax is the maximum index of potentially toxic element pollution, and n is the number of potentially toxic elements. According to PINemerow, soil quality is classified into five levels (Table 9). Based on the obtained PINemerow values, the studied samples were placed in Class 3 and exhibited low pollution levels.

3.4.3.1.4. Contamination Factor (CF)

This factor is used to measure the values of elements in relation to their natural values and to determine the level of soil contamination.

$$CF = \frac{C_m}{Cp_{-i}} \quad \text{(Eq. 4)}$$

Where Cm is the average amount of pollutant or potentially toxic element in the samples, and Cp-i is the amount of pollutant or potentially toxic element in the reference sample. The contamination factor is classified into four grades to monitor the pollution levels of specific metals over time. The contamination levels can be classified based on their intensities on a scale ranging from 1 to 4. They are classified as 1 (< 1) = low, 2 (1-3) = moderate, 3 (3-6) = considerable, and 4 (> 6) = very high (Kowalska et al., 2018).

3.4.3.1.5. Pollution Load Index (PLI)

This index is also used to evaluate the overall level of soil pollution. The PLI provides an easy way to demonstrate soil degradation due to the accumulation of potentially toxic elements (Kowalska et al., 2018). PLI is calculated using the following formula:

$$PLI = \sqrt[n]{Cf_1 x Cf_2 x Cf_3 x \ldots x Cf_n} \quad \text{(Eq. 5)}$$

3.4.3.1.6. Geo-accumulation Index (I_{geo})

A standard method for estimating soil contamination with potentially toxic elements is to obtain the concentration of these elements in the soil relative to the metal reference concentration using the Igeo index introduced by Müller (1969).

$$I_{geo} = \log_2(Cn / 1.5Bn) \qquad \text{(Eq. 6)}$$

Igeo is the geochemical accumulation index or pollution intensity index, Cn is the potentially toxic element concentration in the soil, and Bn is the reference concentration. A factor of 1.5 is introduced to minimize possible variations in the background values attributed to lithologic differences in the soils (Muller, 1969). These variations are generally attributed to changes in soil lithology and the influence of human factors. By separating the natural fluctuations in the concentration of a particular substance in the environment, this coefficient reveals even tiny changes caused by human intervention (Khodaverdiloo et al., 2012). Muller (1969) proposed that the descriptive classes for increasing Igeo levels can be classified based on their intensities on a scale ranging from 1 to 6. They are classified as follows:

0 = unpolluted, 1 = unpolluted to moderately polluted, 2 = moderate, 3 = moderately to strongly polluted, 4 = strongly polluted, 5 = strongly to extremely polluted, and 6 = extremely polluted.

3.4.3.1.7. Sum of Pollution Index (PI_{sum})

This index has several applications in evaluating the quality of soil and deposits concerning heavy elements. Here, PI is the index of potentially toxic element pollution, and n is the number of investigated metals. Accordingly, the total pollution index is calculated as follows

$$PI_{sum} = \sum_{i=1}^{n} PI \qquad \text{(Eq. 7)}$$

or

$$PI_{sum} = PI_{Se} + PI_{As} + PI_{Ca} + PI_{Mg} + PI_{Cd} + PI_{Co} + PI_{Cr} + PI_{Cu} + PI_{Mn} + PI_{Mo} + PI_{Ni} + PI_{Pb} + PI_{Zn} + PI_{Fe} + PI_{V} \quad \text{(Eq. 8)}$$

3.4.3.1.8. Average of Pollution Index (PI_{avg})

This index, first used by (Gong et al., 2009; Inengite et al., 2015) to evaluate soil quality, is calculated using the following formula.

$$PI_{avg} = 1/n \sum_{i=1}^{n} PI \quad \text{(Eq. 9)}$$

Where n is the number of potentially toxic elements under study, and PI_{avg} is the average pollution index. The PI_{avg} values above 1.00 indicate low soil quality and severe pollution (Inengite et al., 2015).

3.4.3.1.9. Vector Modulus of Pollution Index (PI_{Vector})

PI_{vector} is used more frequently than the other indices. In this index, the most severe element of pollution carries more weight because it is squared, making it more realistic (Kowalska et al., 2018). Here, n represents the number of potentially toxic elements considered.

$$PI_{vector} = \sqrt{\frac{1}{n}\sum_{i=1}^{n}(PI)^2} \quad \text{(Eq. 10)}$$

Based on the obtained PI_{vector} values, As is a polluting element in the study area.

3.4.3.1.10. Degree of contamination (Cdeg)

Pollution can be assessed using the C_{deg} index presented by Hakanson (1980). This index is calculated as follows:

$$C_{\deg} = \sum_{i=1}^{n} C_f \quad \text{(Eq. 11)}$$

Where C_f is the pollution factor, and n is the number of considered potentially toxic elements. Kowalska et al (2018) divided the contamination factors into four groups based on the severity of the contamination. They were classified as follows: < 8 = low degree of contamination; 8 to 16 = moderate degree of contamination; 16 to 32 = considerable degree of contamination; and > 32 = very high degree of contamination.

3.4.3.1.11. Multi-element contamination (MEC)

MEC was introduced by Adamu and Nganje (2010) to evaluate pollution based on the concentration of potentially toxic elements in surface soil horizons. To this end, the boundaries presented by Kloke (1983) in Table 18 are utilized.

MEC values greater than 1.00 indicate human-induced effects on the concentration of potentially toxic elements in the soil. MEC is calculated using the following formula:

$$MEC = \frac{\frac{c_1}{T_1} + \frac{c_2}{T_2} + \frac{c_3}{T_3} + \cdots \frac{c_n}{T_n}}{n} \quad \text{(Eq. 12)}$$

Where C represents the amount of potentially toxic elements, T denotes the tolerable levels presented by Kloke (1983) in Table 2, and n indicates the number of potentially toxic elements.

Table 2. MEC index for assessing pollution based on the content of potentially toxic elements in the surface horizons of soil (Kloke, 1983).

Potentially toxic elements	As	Pb	Ni	Zn	Cd	Cr	Cu
Tolerable Levels	20	100	50	300	3	100	100

The MEC values were below 1 for all examined samples, indicating a lack of human impact on the concentrations of potentially toxic elements in the soil.

3.4.3.1.12. Modified degree of contamination (MCd)

This index was proposed by Abrahin and Parker (2008) to evaluate the contamination of the entire soil with potentially toxic elements. It is calculated using the total content of these elements. MCd is determined using the following formula:

$$MCD = \sum_{i=1}^{n} C_{i} / n \quad \text{(Eq. 13)}$$

Where n is the number of analyzed potentially toxic elements, and C_i is the concentration of these elements. The value of pollution is divided into seven groups based on the modified degree of pollution (Kowalska et al., 2018). They are classified as follows: < 1.5 = very low, 1.5 to 2= low, 2 to 4= moderate,4 to 8= high,8 to 16= very high, 16 to 32= extremely high, and > 32 = ultra-high.

4. Results and discussion

4.1. Alteration processes in the study area

The granitoid rocks of the Chore Nab area, which intrude into Eocene-aged volcanic rocks, have significantly influenced the region's mineralization and alteration processes (Nabatian et al., 2014). These volcanic rocks, including basalt, basalt andesite, trachybasalt, and dacite, along with pyroclastic deposits such as crystalline tuff and small tuffs, have undergone extensive alteration, primarily due to the thermal effects of the intruding granitoid mass and the associated hydrothermal fluids. Notably, mineralization has primarily occurred in granitoid rocks. Field evidence and petrographic studies indicate that the alteration process has taken place differently in the Chore Nab region. In some instances, it has led to the formation of one or more minerals in the form of veins or veinlets, or as fillings in cavities within the studied rocks. At times, it has affected the entire rock, and in other cases, it has caused the alteration of one or more minerals. This alteration process is reflected in the mineralogical changes observed in the region, where amphiboles and biotite have been transformed into chlorite, pyroxenes into epidote, and feldspars into sericite. Alteration has affected plutonic rocks (e.g., monzonite and monzonite quartz) and volcanic rocks (including basaltic rocks). The green color of the rocks in the study area is due to alteration minerals such as actinolite, chlorite, and epidote. The observed alterations include epidotization, chloritization, sericitization, carbonatization, silicification, and goethitization. Sericite is the result of the decomposition of feldspars, especially plagioclase. Based on the XRD results (Table 3), the studied rocks, including

plutonic and volcanic rocks, show some alteration. Zoisite, a hydrous silicate containing calcium (Ca) and aluminum (Al), forms from the alteration of plagioclase in granitoid and volcanic rocks. Sericite in plutonic and volcanic rocks is the product of the decomposition of feldspars and plagioclase, respectively. Sericitization has occurred more intensively in plutonic rocks than in volcanic rocks. Chloritization has occurred in both plutonic and volcanic rocks. In this process, chlorite is mainly the result of the decomposition and alteration of mafic minerals, especially amphibole and biotite. During the epidotization process, plagioclases in granitoid and volcanic rocks have decomposed into epidote. In addition, as a result of this process, epidotes are formed on the fracture surfaces of the studied igneous rocks and in the cavities of volcanic rocks. Carbonatization was observed in the studied rocks in the form of calcite veins and veinlets or through the decomposition of plagioclase into calcite. Sericitization is more common in dacitic rocks, while chloritization occurs in granitoid rocks, volcanic rocks, and ore bodies. Epidotization is manifested as epidote veins and veinlets in the igneous rocks of the region, including both plutonic and volcanic rocks. Additionally, it appears as filling cavities in volcanic rocks or as alteration of mafic and plagioclase minerals. Epidote group minerals (mainly zoisite and clinozoisite) are products of the decomposition and alteration of pyroxenes and amphiboles (Hunstman, 1984). Carbonatization, in the form of veins and veinlets, has occurred in the igneous rocks of the region, including both plutonic and volcanic types; in some cases, it has filled cavities in volcanic rocks.

Table 3. Phases identified in the samples based on X-ray diffraction analysis.

Sample Number	Rock Name	Major minerals	Minor minerals	Texture	Altration Minerals	Fe-Ore
Ch-40	Quartz Monzonite	Orthoclase Quartz Albite	Diopside Actinolite Biotite	Granular	Epidote Chlorite Calcite Zoisite	Magnetite Hematite
Ch-51	Quartz MonzoDiorite	Quartz Orthoclase Oligoclase	Biotite Actinolite	Granular	Epidote Calcite Sericite	Magnetite Goethite
Ch-71	Quartz MonzoDiorite	Quartz Orthoclase Oligoclase	Diopside Biotite Muscovite	Granular	Epidote Chlorite Sericite Calcite	Magnetite Hematite Goethite
Ch-74	Diorite	Quartz Andesine	Biotite Actinolite Diopside Zircon	Granular Inter Granular	Epidote Chlorite Calcite Zoisite	Magnetite
Ch-82	MonzoDiorite	Orthoclase Oligoclase Quartz	-	Granular	Epidote Chlorite Sericite Calcite Zoisite	Magnetite Hematite Goethite

Ch-41	Basalt	Anorthite Diopside	Olivine Biotite	Porphyry Glomero Porphyry	Epidote Chlorite Calcite Muscovite Zoisite	Magnetite Hematite
Ch-43	Trachy-andesite	Anorthite Diopside	Actinolite	Porphyry Hyalo- Porphyry	Epidote Chlorite Calcite Muscovite	Magnetite
Ch-48	Andesite-basalt	Augite Labradorite	Kaolinite Montmorillonite Biotite Spinel	Porphyry	Epidote Chlorite	Magnetite Hematite
Ch-53	Andesite	Andesine Hornblende	Actinolite Biotite	Porphyry	Epidote Chlorite	Magnetite
Ch-78	Dacite	Quartz Sanidine Labradorite	Biotite	Porphyry	Epidote Chlorite Calcite Zoisite Sericite	Magnetite Hematite

4.2. Statistical analyses

4.2.1. Correlations between geochemical parameters

Considering the presence of LOI in the samples and the need to normalize the data, Pearson's correlation coefficient was calculated using SPSS software for pairs of elements relative to each other. This coefficient measures the correlation between two random variables whose values vary between -1 and +1. Here, +1 indicates the highest positive correlation between two variables, -1 denotes the highest inverse correlation of the variables, and 0 means a lack of any correlation. In calculations, the correlation coefficient of each element is equal to one. In this study, the examined samples are classified according to the following system:

0 to 0.2: Weak correlation

0.2 to 0.69: Average correlation

0.69 to 1: Strong correlation

Bivariate statistical techniques, such as the correlation coefficient, are beneficial for reviewing the paragenetic relationships between various elements and determining their sources. Pearson's correlation coefficient between two variables is defined as the covariance of the two variables divided by the product of their standard deviations. The bivariate Pearson correlation coefficient indicates both the strength and nature of the relationship, whether direct or inverse. The correlation coefficients between the elements are presented in Table 4. According to the calculated correlation coefficients, Fe has a positive correlation with Mo (0.177) and a negative correlation with Cu (-0.238). Additionally, manganese (Mn) has a positive correlation with lead (0.072), zinc (0.045), and chromium (0.147). This issue may be due to the different absorptions of these elements by Fe and Mn oxides and hydroxides. The results show a positive correlation of Ni with Cr (0.035) and Co (0.876), V with Co (0.587), Zn with Cu (0.154), and Zn with Pb (0.167). These data can be attributed to the same origin of these elements, the presence of these elements in the structure of sulfide minerals, or the similar geochemical behavior of these elements in relation to one another. The negative correlation of As with Mn (-0.413), Mo (-0.188), and Zn (-0.039) indicates that the abundance of these elements is not related to arsenic.

Table 4. Calculation of the correlation coefficients of elements relative to each other.

	As	Ca	Mg	Cd	Co	Cr	Cu	Mn	Mo	Ni	Pb	Zn	Fe	V
As	1													
Ca	0.927*	1												
Mg	-0.413	-0.451	1											
Cd	0.603*	0.481	0.094	1										
Co	0.016	-0.009	0.702**	0.604*	1									
Cr	0.420	0.381	-0.408	0.171	-0.029	1								
Cu	0.487	0.397	0.172	0.982**	0.666**	0.107	1							
Mn	0.227	0.218	-0.228	-0.107	-0.502	0.147	-0.145	1						
Mo	-0.188	0.158	0.358	-0.084	0.399	-0.077	-0.042	-	1					
Ni	0.334	0.281	0.442	0.818**	0.876**	0.035	0.827**	-	0.269	1				
Pb	0.574*	0.540*	0.019	0.811**	0.390	0.133	0.805**	0.0	0.230	0.565*	1			
Zn	-0.039	-0.236	0.661*	0.187	0.264	-0.443	0.154	0.0	-	0.292	0.167	1		
Fe	0.262	0.232	-0.171	-0.024	0.133	0.467	-0.238	0.1	0.177	0.087	0.154	-0.330	1	
V	0.794*	0.724**	0.131	0.865**	0.587*	0.290	0.811**	-	0.099	0.793**	0.746**	0.188	0.413	1

**Correlation is significant at the 0.1 level

* Correlation is significant at the 0.05 level

4.2.2. Principal Component Analysis (PCA)

Factor analysis is a method used to study the intended variable changes at one point and the reflection of the changes simultaneously (Davis and Sampson, 1986; Ghassemi Dehnavi et al.,2019; Mokarram et al., 2020; Negahban and Mokarram, 2021; Sikakwe and Ilaumo, 2023). PCA is one of the multivariate statistical methods that can be used to reduce the complexity of variable analysis and provide a better interpretation of large volumes of information and data (Dabiri et al., 2017). In this study, PCA was conducted to identify the sources of contamination, and both PCA and HCA were used to distinguish between the different groups of elements. Based on the results of PCA, the analyzed element contents are grouped into a three-component model (PC1, PC2, and PC3). Table 5 shows the summary of the statistical results of potentially toxic elements in the soil of the study area. The PCA results of the potentially toxic elements studied in the area are illustrated in Table 6. PC1 described 43.34% of the total data variability, showing maximum positive loadings for Cd (0.948), Fe (0.720), Ni (0.808), Cu (0.910), Co (0.592), As (0.741), Pb (0.837), Ca (0.646) and V (0.968). However, it reflected moderate and low positive loadings for Fe (0.720), As (0.741), and Co (0.592), respectively. PC2 accounted for 23.52% of the total data variability, showing maximum positive loadings for Zn (0.855) and Mg (0.792) and negative loadings for Cr (-0.692) and Ca (-0.544). PC3 describes 10.84% of the total data variability, showing maximum positive load for Co (0.661) and Mo (0.745) and negative loading

for Mn (-0.823). The analyzed element contents are grouped into a three-component model that accounts for 77.70% of the total variance. Definitely, the elements that are in the same component have a common origin in lithology or chemical dependency. These results are compatible with those obtained from the Pearson coefficient. The same origins cause the aggregation of some elements together. In other words, the origin of the first component's elements can be attributed to lithological activities; the second component's elements to the weathering and alteration of mafic rocks such as basalt and andesite basalt; and the third component's elements to the weathering and alteration of granitoid rocks.

4.2.3. Cluster analysis (CA)

Cluster analysis is a multivariate method used for grouping samples and variables based on the similarity of characteristics and origin. Clustering is selected based on maximum inter-cluster similarity and minimum intra-cluster similarity (Potashev et al.,2014; Sarikhani et al., 2021;Islam et al., 2024). Cluster analysis (CA) is a multivariate technique for analyzing correlation coefficients to obtain similarity coefficients and to plot a dendrogram. Cluster analysis of potentially toxic elements and the cluster analysis of sampling points are shown in Figs. 19 and 20, respectively. Additionally, the loading plots of the components are illustrated in Fig. 21. The results of the Pearson coefficients are also confirmed by a cluster analysis. Based on the results of the HCA analysis (Fig. 19), four different clusters were identified. The first cluster includes two subgroups. The first subgroup consists of the elements Mo, Cd, As, Ni, Co, Cr, Zn, V, Cu, and Pb (which are very similar and correlated) and Mn (which, despite its slight difference from the other elements, is included in the first subgroup). The second subgroup contains the element Se. The second cluster includes the element Ca, the third cluster includes the element Fe, and the fourth cluster includes the element Mg. Differences in groups of elements indicate different origins for the elements. Grouping the mentioned elements into a major branch can be related to their geological origin and mining activities. Therefore, these analyses suggest that the studied elements could be classified from Group 1 (G1) to Group 4 (G4) concerning source identification. Consequently, it can be concluded that these elements originate from natural sources. Cluster 1, Cluster 2, Cluster 3 and Cluster 4, indicating similar characteristic features of pollution, may be related to weathering and alteration activities.

4.2.4. Scree plot

The Scree plot is a brief and easily applicable test for determining the number of extracted factors in factor analysis experiments, as proposed by Cattell (1966). The scree plot illustrates the importance of each factor based on the total variance and confirms the eigenvalues table. In this diagram, the vertical axis represents the specific values of the components, while the horizontal axis indicates the component numbers. In Fig. 22, it is observed that the first three components have eigenvalues greater than 1, while from the fourth component onward, the eigenvalues are less than 1. This indicates the presence of three effective factors in the samples and confirms the PCA results.

Table 5. Summary statistics of potentially toxic elements in the soil of the study area.

Variable	Minimum	Maximum	Mean	Variance	Std Dev
Ni	7	28	12.29	5.483	30.066
Co	4.0	27.5	13.914	6.1348	37.635
Zn	21	218	92.93	45.987	2114.841
Cr	14	229	68.21	64.816	4201.104
Se	5000	5000	5000.00	.000	.000
As	.7	20.9	4.250	6.4068	41.047
Ca	21817	91666	37598.00	18699.932	349687442.923
Cu	6	712	86.29	181.794	33048.989
Fe	30589	80009	48517.36	14729.529	216959011.632
Mg	2710	17407	13579.14	4317.750	18642969.055
Mn	373	2721	1441.86	692.315	479300.286
Mo	.51	1.08	.7371	.16923	.029
Pb	15	53	24.07	10.716	114.841
V	57	402	156.57	84.169	7084.418
Cd	.20	1.40	.3243	.31137	.097

Table 6. Principal Component Analysis of potentially toxic elements.

Variable	PC1	PC2	PC3
Ni	.808		
Co	.592		.661
Zn		.855	
Cr		-.692	

As	.741		
Ca	.646	-.544	
Cu	.910		
Fe	.720		
Mg		.792	
Mn			-.823
Mo			.745
Pb	.837		
V	.968		
Cd	.948		
Total	6.068	3.293	1.518
% of Variance	43.344	23.521	10.843
Cumulative %	43.344	66.865	77.708

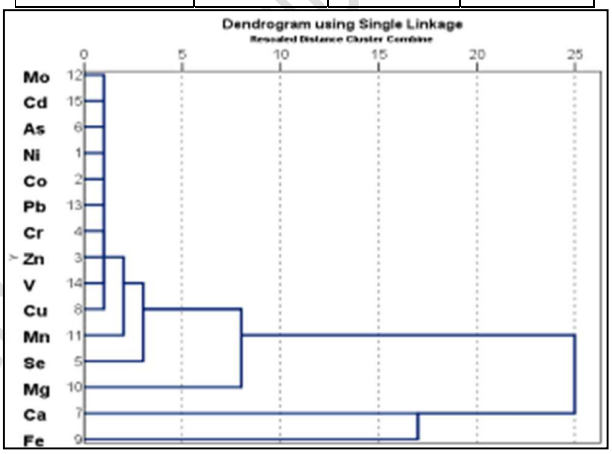

Figure 19. Cluster analysis of potentially toxic elements in the soils of the study area.

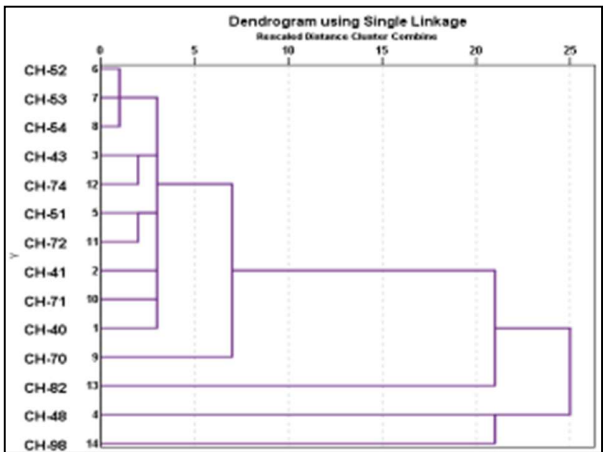

Figure 20. Cluster analysis of sampling points in the soils of the study area.

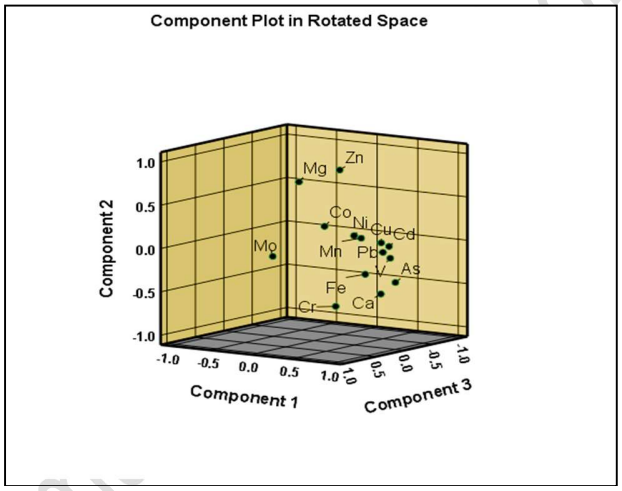

Figure 21. Loading plot of analyzed elements in the space described by three principal components (PC1, PC2, and PC3).

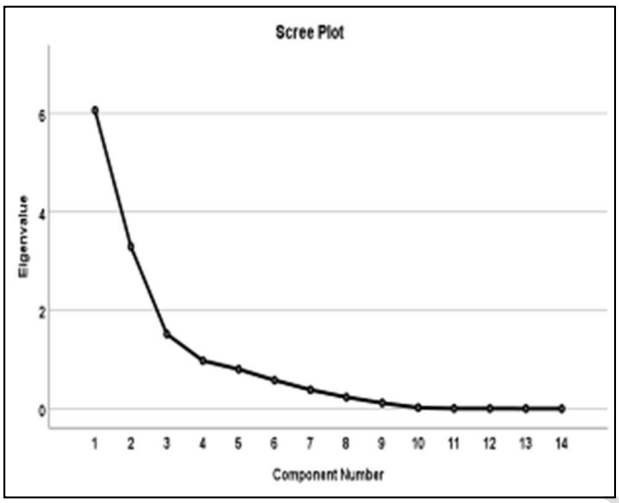

Figure 22. Scree plot related to sampling elements.

4.2.5. Quantitative calculations of pollution assessment

Based on the EF calculated for 15 elements, it was determined that only Arsenic (6.50) has significant enrichment or significant contamination. Other components have minimal pollution, while Cd (2.74), Cr (2.38), and Mn (2.45) show moderate enrichment. The type of pollution is determined according to Table7 . According to the EF diagram, it was also found that arsenic (As) has the highest degree of contamination in the study area (Fig. 23). According to the PI values, Arsenic (3.86) is the only element with severe pollution in the region, while the values of Se, Ca, Cd, Cr, Cu, Mn, Pb, and Zn vary in the ranges of 1.00,1.00, 1.54,1.41, 1.02,1.44, 1.09, and 1.12, respectively (Table 8). According to $PI_{Nemerow}$, all studied samples fall into Class 3 and show little pollution (Table 9). The results of I_{geo} calculated for different elements show only Arsenic (1.36) with moderate pollution, while other components have not polluted the Chore Nab area (Table 10). However, the pollution load index (PLI) indicates unfavorable soil quality (Table 11). Based on the PI_{vector} values, Arsenic (1.43) is a polluting element in the study area (Table 12). Based on the MCd values (Table 13), most samples have a high degree of contamination, and Sample CH-48 has a very high degree of contamination. According to the investigated pollution indices, the area's pollution has a natural origin, and human activities have not affected the pollution of the study area. From an environmental perspective, the enrichment of certain elements, particularly arsenic (As), chromium (Cr), and manganese (Mn), in the Chore Nab area poses significant ecological concerns. This is corroborated by the pollution index (PI) values, which reveal severe arsenic contamination in the region. The pollution load index (PLI) results further underscore the poor soil quality in the area. While the natural origin of the pollution is evident, the potential risks to the environment and public health cannot be overlooked. This is particularly relevant in the context of similar studies, where natural geogenic sources have been identified as significant contributors to the contamination of potentially toxic elements (Mishra et al., 2019). The results of the contamination factor (CF) and degree of contamination (Cdeg) indicate significant arsenic pollution in the region. The findings are presented in Tables 14 and 15.

Table 7. Enrichment coefficient index values (Kowalska et al., 2018).

EF Value	Enrichment of soil
< 2	deficiency to minimal enrichment
2-5	moderate enrichment
5-20*	significant enrichment
20-40	very high enrichment
> 40	extremely high enrichment

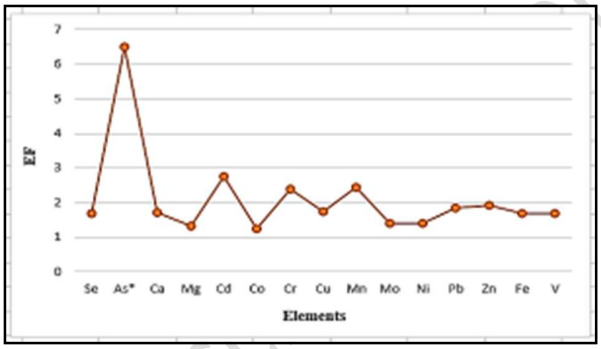

Figure 23. Linear diagram of the enrichment factor of potentially toxic elements in the studied samples.

Table 8. Pollution class based on the pollution index (Kowalska et al., 2018).

Class	Value of PI	Soil pollution
1	PI <1	absent
2	1< PI< 2	low
3	2< PI< 3	moderate
4	3< PI< 5	strong
5	PI >5	very strong

Table 9. Soil quality based on the Nemerow pollution index (Kowalska et al., 2018).

Class	Value of $PI_{Nemerow}$	Quality of soil
1	≤ 0.7	Clean
2	0.7-1	Warning limit
3*	1-2	Slight pollution
4	2-3	Moderate pollution
5	≥ 3	Heavy pollution

Table 10. Soil quality based on the geo-accumulation index (Muller, 1969)

Class	Values of I_{geo}	Soil quality
0	I ≤ 0	unpolluted
1	0-1	unpolluted to moderately polluted
2	1-2	moderately polluted
3	2-3	moderately to highly polluted
4	3-4	highly polluted
5	4-5	highly to extremely high polluted
6	5-6	extremely high polluted

. Table 11. Pollution class based on pollution load index Kowalska et al., 2018

Class	PLI	Quality of soil
1	< 1	denote perfection
2	1	only baseline levels of pollution
*3	> 1	deterioration of soil quality

Table 12. Vector modulus of the pollution index calculated for the examined elements.

Elements(ppm)	Value of $(PI_{Vector})^2$	PI_{Vector}
Se	1	
As*	14.90	
Ca	1.00	
Mg	0.6	
Cd	2.32	
Co	0.518	
Cr	1.99	
Cu	1.04	
Mo	2.07	
Ni	0.39	
Pb	0.65	
Zn	1.18	
Fe	1.34	
Mn	0.98	1.43
V	0.96	

Table 13. Corrected degree of pollution for the studied samples.

Sample	M_{Cd}	Degree of contamination
Ch-40	6.42	high
Ch-41	6.46	high
Ch-43	6.60	high
* Ch-48	12.041	very high
Ch-51	6.09	high
Ch-52	7.36	high
Ch-53	6.009	high
Ch-54	7.22	high
Ch-70	4.50	high
Ch-71	5.74	high
Ch-72	6.004	high
Ch-74	6.57	high
Ch-82	7.96	high
Ch-98	6.41	high

Table 14. Calculated contamination factor for the studied samples.

Element	Value of C_f	Soil pollution
Se	1	moderate contamination
As*	3.86	considerable contamination *
Ca	1.005	moderate contamination
Mg	0.78	low contamination
Cd	1.62	moderate contamination
Co	0.74	low contamination
Cr	1.42	moderate contamination
Cu	1.02	moderate contamination
Mn	1.44	moderate contamination
Mo	0.79	low contamination
Ni	0.82	low contamination
Pb	1.09	moderate contamination
Zn	1.13	moderate contamination
Fe	1.001	moderate contamination
V	0.98	low contamination

Table 15. Calculation of the pollution degree in the studied samples.

C_{deg}	Contaminants
18.56	considerable degree of contamination

Conclusion

This study provides a comprehensive evaluation of the alteration zones, pollution indices, and environmental impacts of potentially toxic elements in the Chore Nab iron mine. The findings highlight that the granitoid rocks of the study area, which intruded into Eocene volcanic rocks, have undergone significant alteration processes. In the Chore Nab region, six alteration zones were identified based on a thorough methodology involving petrographic analysis and geochemical studies. Field observations provided initial indications of alteration features such as veins, veinlets and color changes, which were then examined in detail through petrographic analysis to observe mineralogical transformations. Geochemical analysis further supported the identification of these zones by quantifying element concentrations associated with alteration processes. The integration of these data allowed us to classify and distinguish the alteration zones into six categories: epidotization, chloritization, sericitization, carbonatization, silicification, and goethitization, each defined by distinct mineralogical and geochemical characteristics.

These alterations have led to the formation of various minerals, including actinolite, particularly within the monzonite and volcanic rocks, contributing to environmental pollution in the region. During the study, we found significant positive correlations between Co and Ni (0.876), V and Ni (0.793), Mg and Co (0.704), Cu and Cd (0.982), and Cu and Pb (0.805), which indicate the same origin of these elements, the presence of these elements in the structure of sulfide minerals, or the similar geochemical behavior of these elements concerning each other. According to the results obtained from the bio-environmental analyses, including the enrichment factor (EF), pollution index (PI), and geoaccumulation index (Igeo), arsenic (As) is identified as the primary contaminant, exhibiting significant enrichment, severe pollution levels, and moderate pollution in the area, respectively. Additionally, cadmium (Cd), chromium (Cr), and manganese (Mn) show moderate enrichment. The contamination in the region is predominantly of natural origin, with minimal influence from human activities. The current study shows that the soils are contaminated with certain harmful toxic elements. Assessing the correlation based on the Pearson factor and principal component analysis revealed that the distribution of elements such as Cd, Fe, Ni, Cu, As, Pb, Ca, V, and Co is controlled by lithological sources, whereas the distribution of Zn and Mg is influenced by the weathering and alteration of mafic rocks. In general, the investigation of the relationship between the obtained data and the geology of the study area demonstrates that the origin of these element concentrations is geogenic and related to mineralization and alteration. This research provides a detailed assessment of the environmental impact of alteration processes in mining regions, particularly regarding the pollution of potentially toxic elements. The findings underscore the importance of monitoring and managing natural sources of pollution to mitigate their impacts on the environment and human health.

References

Abdolahadi A., Sheikhzakariaee S.J., Yazdi A., Mousavi S.Z. (2025) Plio-Quaternary Adakite Genesis and Post-collisional Processes: Whole Rock Constraints and Sr, Nd Isotopic Compositions in Alborz Magmatic Belt, Ardabil, Iran. *Journal of Mining and Environme*nt 16(2):737-765. DOI: https://doi.org/10.22044/jme.2024.14781.2801

Abdullah M.Z., Louis V.C., Abas M.T. (2015) Metal pollution and ecological risk assessment of Balok River Sediment, Pahang Malaysia. *American Journal of Environmental Engineering,* 5(3A), pp. 1-7.

Abrahim G.M.S., Parker R.J. (2008) Assessment of heavy metal enrichment factors and the degree of contamination in Marine Sediments from Tamaki Estuary, Auckland, New Zealand. *Environmental Monitoring and Assessment,* 136, 227-238.https://doi.org/10.1007/s10661-007-9678-2

Adamu C.I., Nganje T.N. (2010) Heavy metal contamination of surface soil in relationship to land use patterns: a case study of Benue State, Nigeria. *Materials Sciences and Applications,* 127-134. https://doi.org/ 10.4236/msa.2010.13021

Agyeman P.C., John K., Kebonye N.M., Boruvka L., Vasat R. (2023) Combination of enrichment factor and positive matrix factorization in the estimation of potentially toxic element source distribution in agricultural soil. *Environmental Geochemistry and Health,* 45(5), 2359-2385. https://doi.org/10.1007/s10653-022-01348-z

Amini B. (1997) Geological Map 1:100000 of Tarom. Organization of Geology and Mineral Exploration of the Country.

Atabaki M.R., Lotfi A. (2018) Investigation of soil heavy metals concentrations (Pb, Cd, Zn and Cu) in different areas of Isfahan. *Journal of Research in Environmental Health,* Volume 4, Issue 1, 23-35 (in Persian). https://doi.org/10.5923/c.ajee.201501.01

Azami J., Taban P. (2018) Monitoring of potentially toxic elements in water, sediment and phragmites Australis - Of Aras River along the Iranian- Armenian Border. *Iranian Journal of Toxicology,* 12(2). 1-6(in Persian).

Bain W.M., Steele-MacInnis M., Li K., Li L., Mazdab F.K., Marsh E.E. (2020) A fundamental role of carbonate–sulfate melts in the formation of Iron Oxide–Apatite Deposits. *Nature Geoscience,* 13(11),751-757. https://doi.org/10.1038/s41561-020-0635-9

Biabangard H., Boomeri M., Taimouri K., Mohammadpour F. (2017) Petrography, alteration and genesis of Iron Mineralization in Roshtkhar. *Journal of Economic Geology,* 9(1), 93-115. https://doi.org/10.22067/ECONG.V9I1.47297

Bonyadi Z., Sadeghi R. (2020) Hydrothermal alteration associated with magnetite mineralization in the Bafq Iron Deposits, Iran. *Journal of Asian Earth Sciences,* 189, 104152. https://doi.org/10.1016/j.jseaes.2019.104152

Cattell R.B. (1996) The Scree test for the number of factors. *Multivariate Behavioral Research.* 1966 Apr 1; 1(2): 245-76. https://doi.org/10.1207/s15327906mbr0102_10

Chowdhury S., Lentz D. R., Pal D.C. (2024) Hydrothermal alteration and elemental mass balance for the Surda Copper Deposit, Singhbhum Shear Zone, Eastern India: Implications for both Copper and Magnetite–Apatite Mineralization. *Geochemistry: Exploration, Environment, Analysis,* 24(3). https://doi.org/10.1144/geochem2024-004

Dabiri R., Bakhshi Mazdeh M., Mollai H. (2017) Heavy metal pollution and identification of their sources in soil over Sangan iron-Mining Region, NE Iran. *Journal of Mining and Environment* 8(2): 277-289. https://doi.org/10.22044/jme.2016.820

Davis J. C., Sampson R.J. (1986) Statistics and data analysis in geology, Wiley New York.

De Oliveira S.M.B., Imbernon R.A.L. (1998) Weathering alteration and related REE concentration in the Catalão I Carbonatite Complex, Central Brazil. *Journal of South American Earth Sciences,* 11(4), 379-388.

Evans L.J. (1992) Alteration products at the earth's surface, the clay minerals. *Developments in Earth Surface Processes,* 2, 107-125. https://doi.org/10.1016/B978-0-444-89198-3.50010-6

Fan Y., Zhang W., Liu Y., Zhou T., Zhang L., Chen X., Hong H. (2021) Geochemical characteristics of chlorite in the Luohe iron deposit in the Middle-Lower Yangtze Metallogenic Belt, Eastern China. *Ore Geology Reviews,* 133, 104062. https://doi.org/10.1016/j.oregeorev.2021.104062

Ghassemi Dehnavi A., Sarikhani R., Moradpour A., Amiri M. (2019) Distribution and source identification of heavy metals in the soil surrounding Kermanshah Refinery, Iran. *Journal of Advances in Environmental Health Research* 7, no. 3. 169-177. https://doi.org/ 10.22102/JAEHR.2019.165070.1120

Gong Q., Deng J., Xiang Y., Wang Q., Yang L. (2009) Calculating pollution indices by heavy metals in ecological geochemistry assessment and a case Study in Parks of Beijing. *Journal of China University of Geosciences,* 19, 230–241.

Hakanson L. (1980) An ecological risk index for aquatic pollution control. *A Sedimentological Approach, Water Research,* Volume 14, Issue 8, Pages 975-1001. https://doi.org/10.1016/0043-1354(80)90143-8

Hirayama K., Samimi M., Zahedi M., Hushmand-Zadeh A. (1966) Geology of the Tarom district, Western Part (Zanjan Area, Northwest Iran). *Geol. Surv. Iran, Rep*. 8, 31 p.

Huntsman J.R. (1984) Caribou Mountain; a porphyry copper deposit in Southeastern Idaho. *Economic Geology,* 79(4), 748-754. https://doi.org/10.2113/gsecongeo.79.4.748

Inengite A.K., Abasi C.Y., Walter C. (2015) Application of pollution indices for the assessment of heavy metal pollution in Flood Impacted Soil. *International Research Journal of Pure & Applied Chemistry,* 8(3): 175-189, ISSN: 2231-3443. https://doi.org/10.9734/IRJPAC/2015/17859

Islam S., Sarker M.E., Hoque M.M.M., Kabir M.H., Ahmed F.T., Hossain M.N. (2024) Quantification of heavy metals concentration and assessment of ecological health risk in roadside agricultural land of Dhaka-Aricha Highway, Bangladesh. *Iranian Journal of Earth Sciences,* 16(1), 1-12. https://doi.org/10.57647/j.ijes.2024.1601.01

Kabata-Pendias A. (2011) Trace elements of soils and plants. *Boca Raton: CRC press, Taylor &Francis Group,* (4th ed., pp. 28–534).

Khodaverdiloo H., Ghorbani Dashtaki S.h. (2012) A brief survey of metal-accumulated plants and their host soils in Iran. *Journal of Environment Science,* 51: 3-12 (in Persian).

Kloke A. (1983) Tolerable amounts of heavy metals in soil and their accumulation in plants. environmental effects of organic and inorganic contaminants in Sewage Sludge, *Scientific Research,* 171-175.

Kowalska J.B., Mazurek R., Gasiorek M., Zaleski T. (2018) Pollution indices as useful tools for the comprehensive evaluation of the degree of soil contamination–A review. *Environ Geochem Health,* Volume 40, pages 2395-2420. https://doi.org/10.1007/s10653-018-0106-z

Kumar V., Parihar R.D., Sharma A., Bakshi P., Sidhu G.P.S., Bali A.S., Rodrigo-Comino J. (2019) Global evaluation of heavy metal content in surface water bodies: a meta-analysis using heavy metal pollution indices and multivariate statistical analyses. *Chemosphere,* 236,124364.https://doi.org/10.1016/j.chemosphere.2019.124364

Leitch C.H.B., Lentz D.R. (1994) The gresens approach to mass balance constraints of alteration systems—methods, Pit-Falls, examples, *in* alteration and alteration processes associated with Ore-Forming Systems. *Geological Association of Canada Short Course Notes,* v. 11, p. 161–192.

Lentini P., Zanoli L., Granata A., Signocelli S.S., Castelino P., Dell Aquila R. (2017) Kidney and heavy metals- the role of environmental exposure. *Molecular Medicine Reports,* 15(5), P 3413- 3419. https://doi.org/10.3892/mmr.2017.6389

Li X.C., Fan H.R., Santosh M., Hu F.F., Yang K.F., Lan T.G. (2013) Hydrothermal alteration associated with mesozoic Granite-Hosted Gold Mineralization at the Sanshandao Deposit, Jiaodong Gold Province, China. *Ore Geology Reviews,* 53, 403-421. http://dx.doi.org/10.1016/j.oregeorev.2013.01.020

Matta G., Gjyli L. (2016) Mercury, lead and arsenic, impact on environment and human health. *Journal of Chemical and Pharmaceutical Sciences.* 9. P 718- 725.

Mishra S., Bharagava R.N., More N., Zainith S.,Yadav A., Mani S., Chowdhary P. (2019) Heavy metal contamination: an alarming threat to environment and human health. *Environmental Biotechnology: For Sustainable Future:* 103-125. https://doi.org/10.1007/978-981-10-7284-0_5

Mohebian M., Sobhanardakani S., Taghavi L., Ghoddousi J. (2021) Analysis and potential ecological risk assessment of heavy metals in the surface soils Collected from various land uses around Shazand Oil Refinery Complex, Arak, Iran. *Arabian Journal of Geosciences* 14: 1-16. https://doi.org/10.1007/s12517-021-08349-9

Mokarram M., Saber A., Sheykhi V. (2020) Effects of heavy metal contamination on river water quality due to release of industrial effluents. *Journal of Cleaner Production,* 277, 123380. https://doi.org/10.1016/j.jclepro.2020.123380

Mollai H., Pe-Piper G., Dabiri R. (2014) Genetic relationships between skarn ore deposits and magmatic activity in the Ahar region, Western Alborz, NW Iran. *Geologica Carpathica* 65(3):207-225.

Muller G. (1969) Index of geoaccumulation in sediments of the Rhine River. *Geo Journal*, V.2, p: 108–118.

Münzel T., Hahad O., Daiber A., Landrigan P.J. (2023) Soil and water pollution and human health. What should cardiologists worry about? *Cardiovascular Research,* 119(2), 440-449. https://doi.org/10.1093/cvr/cvac082

Nabatian G., Ghaderi M., Corfu F., Neubauer F., Bernroider M., Prokofiev V., Honarmand M. (2014) Geology, alteration, age, and origin of Iron Oxide–Apatite Deposits in Upper Eocene Qartz Monzonite, Zanjan District, NW Iran. *Miner Deposita* 49:217–234. https://doi.org/ 10.1007/s00126-013-0484-1

Nazari M., Arian M.A., Solgi A., Zareisahamieh R., Yazdi A. (2023) Geochemistry and tectonomagmatic environment of Eocene volcanic rocks in the Southeastern region of Abhar, NW Iran. *Iranian Journal of Earth Sciences* 15(4): 228-247. DOI: https://doi.org/10.30495/ijes.2023.1956689.1746

Neeraj A., Hiranmai R.Y., Iqbal K. (2023) Comprehensive assessment of pollution indices, sources apportionment and ecological risk mapping of heavy metals in agricultural soils of Raebareli District, Uttar Pradesh, India, employing a GIS Approach. *Land Degradation & Development*, 34(1),173-195. https://doi.org/10.1002/ldr.4451

Negahban S., Mokarram M., Pourghasemi H.R., Zhang H. (2021) Ecological risk potential assessment of heavy metal contaminated soils in Ophiolitic formations. Environmental Research 192: 110305. https://doi.org/10.1016/j.envres.2020.110305

Negahban S., Mokarram M. (2021) Potential ecological risk assessment of Ni, Cu, Zn, Cd, and Pb in Roadside Soils. *Earth and Space Science* 8(4): e2020EA001120. https://doi.org/10.1029/2020EA001120

Ousta S.h., Ashja-Ardalan A., Yazdi A., Dabiri R., Arian M.A. (2024) Petrogenesis and tectonic implications of Miocene dikes in the southeast of Bam (SE Iran): Constraints on the development of active continental margin. *Geopersia* 14 (1): 89-111. DOI: https://doi.org/10.22059/geope.2023.364334.648729

Pirajno F. (2008) Hydrothermal processes and mineral systems. *Springer Science & Business Media.*

Potashev K., Sharonova N., Breus I. (2014) The use of cluster analysis for plant grouping by their tolerance to soil contamination with hydrocarbons at the germination stage. *Science of the Total Environment* 485:71-82. https://doi.org/10.1016/j.scitotenv.2014.03.067

Qingjie G., Jun D., Yunchuan X., Qingfei W., Liqiang Y. (2008) Calculating pollution indices by potentially toxic elements in ecological geochemistry assessment and a case study in Parks of Beijing. *Journal of China University of Geosciences,* 19(3), 230–241.

Rae A., O'Brien J., Ramirez E., Bignall G. (2011) The application of chlorite geothermometry to hydrothermally altered Rotokawa Andesite, Rotokawa Geothermal Field. *New Zealand Geothermal Workshop, Proceedings* 21-23, November, Vol. 33, No 8, Auckland, New Zealand.

Robb L.J. (2005) Introduction to ore-forming processes. *Blackwell Science Ltd. a Blackwell Publishing company.*

Saadat S., Ghoorchi M., Dabiri R..(2023) Extracting clay minerals with emphasis on Bentonite in Eastern Iran, using Landsat 8 and ASTER images. *Iranian Journal of Earth Sciences*.15(3):188-194.. DOI: https://doi.org/10.30495/ijes.2023.1973739.1815.

Sabet Aghlidi P., Cheraghi M., Lorestani B., Sobhanardakani S., Merrikhpour H. (2020) Analysis, spatial distribution and ecological risk assessment of arsenic and some heavy metals of agricultural soils, Case Study: South of Iran. *Journal of Environmental Health Science and Engineering,* 18, 665-676. https://doi.org/10.1007/s40201-020-00492-x

Sampaio G.M.S., Pufahl P.K., Raye U., Kyser K.T., Abreu A.T., Alkmim A.R., Nalini Jr H.A. (2018). Influence of weathering and hydrothermal alteration on the REE and δ56Fe composition of iron formation, Cauê Formation, Iron Quadrangle, Brazil. *Chemical Geology,* 497, 27-40. https://doi.org/10.1016/j.chemgeo.2018.08.014

Salehpour S., Arian M.A., Rad A.J., Zarei Sahamieh R., Yazdi A. (2025) Geochemistry and technomagmatic environment of Eocene volcanic rocks in Yuzbashi Chay region, west of Qazvin (Iran). *Iranian Journal of Earth Sciences* 17(1): 1-13. DOI: https://doi.org/10.57647/j.ijes.2025.1701.04

Sarikhani R., Jamshidi A., Ghassemi Dehnavi A. (2021) Salinity, Chemistry, and Quality of Groundwater in Robat-Khorramabad Plain, West of Iran. *Journal of Engineering Geology*, 14(5), pp.85-112.

Schaefer L.N., Kereszturi G., Kennedy B.M., Villeneuve M. (2023) Characterizing lithological, weathering, and hydrothermal alteration influences on volcanic rock properties via spectroscopy and laboratory testing: a case study of Mount Ruapehu Volcano, New Zealand. *Bulletin of Volcanology,* 85(8),43. https://doi.org/10.1007/s00445-023-01657-w

Siani M.G, Lentz D.R. (2022) Lithogeochemistry of various hydrothermal alteration types associated with precious and base metal epithermal deposits in the Tarom-Hashtjin Metallogenic Province, NW Iran: implications for regional exploration. *Journal of Geochemical Exploration* 232: 106903. https://doi.org/10.1016/j.gexplo.2021.106903

Sikakwe G., Ilaumo B. (2023) Contamination of arable topsoil by organic and inorganic pollutants around petroleum products handling facilities. *Iranian Journal of Earth Sciences,* 15(2). https://doi.org/10.30495/ijes.2022.1943042.1663

Simatupang C.A., Santhaweesuk K., Strezov V., Pongkiatkul P., Boontanon N., Jindal R., Boontanon S.K. (2024) Health risk assessment of soil contamination with heavy metals in a child care center co-located in vicinity to small scale industrial area: Case study of Thailand. *Case Studies in Chemical and Environmental Engineering,* 9, 100727. https://doi.org/10.1016/j.cscee.2024.100727

Sobhanardakani S. (2019) Ecological and human health risk assessment of heavy metal content of atmospheric dry deposition, a case study: Kermanshah, Iran. *Biological Trace Element Research* 187(2): 602-610. https://doi.org/10.1007/s12011-018-1383-1

Stocklin J. (1969) 1:100,000 Geological map of Tarom.

Sutherland R.A. (2000) Bed sediment-associated trace metals in an urban stream, Oahu, Hawaii. *Environmental Geology,* 39, 611–627.

Tajam J., Kamal M.L. (2013) Marine environment risk assessment of Sungai Kilim, Langkawi, Malaysia: Heavy metal. http://dx.doi.org/10.1155/2013/482451

Talaei R., Peyrowan H., Azimi Motem F. (2019) Environmental assessment of contaminated soils in Dostbaiglou Mine (North of Meshginshahr-Iran). *Journal of Natural Environmental Hazards,* Vol.08, Issue 20. https://doi.org/ 10.22111/JNEH.2018.22970.1349

Tomczyk P., Wdowczyk A., Wiatkowska B., Szymańska-Pulikowska A. (2023) Assessment of heavy metal contamination of agricultural soils in Poland using contamination indicators. *Ecological Indicators,* 156,111161. https://doi.org/10.1016/j.ecolind.2023.111161

Torkashvand A., Ghasemi Siani M., Tabbakh Shabani A.A., Karimi Shahraki B. (2019) Environmental impacts of iron ore mining and processing on Chore Nab Fe Ore, Zanjan Province. *The Second Conference on Mining and Green Mining Industries of Iran*(inPersian).

Upadhyay V., Kumari A., Kumar S. (2024) From soil to health hazards: Heavy metals contamination in Northern India and health risk assessment. *Chemosphere,* 354, 141697. https://doi.org/10.1016/j.chemosphere.2024.141697

Whitney D.L., Evans B.W. (2010) Abbreviations for names of rock-forming minerals. *American Mineralogist,* 95(1): 185-187. https://doi.org/10.2138/am.2010.3371

Wu Y., Shen P., Feng H., Li C., Zhao J., Luo Y., Li W. (2024) Textures and chemical compositions of magnetite from Zhibo Submarine Volcanic Iron Oxide Deposit, Xinjiang, China: Implications for Re-Equilibration Processes. *Minerals,* 14(6), 548. https://doi.org/10.3390/min14060548

Yazdi A., Ziaaldini S., Dabiri R. (2015) Investigation on the geochemical distribution of REE and heavy metals in western part of Jalal-Abad iron ore deposit, Zarand, SE of Iran. Open journal of ecology 5(9): 460-476.

Zhang F., Li X., Wei Y. (2023) Selenium and selenoproteins in health. *Biomolecules,* 13(5), 799. https://doi.org/10.3390/biom13050799

Zwolak I., Zaporowska H. (2012) Selenium interactions and toxicity: a review. *Cell Biology and Toxicology* 28: 31-46.